2005

Vibrio cholerae biofilm development on natural and artificial chitin substrates

Mahtab Shahkarami
San Jose State University

NOTE TO USERS

VIBRIO CHOLERAE BIOFILM DEVELOPMENT ON NATURAL AND ARTIFICIAL CHITIN SUBSTRATES

A Thesis

Presented to

The Faculty of the Department on Biological Sciences

San José State University

In Partial Fulfillment

of the Requirements for the Degree

Master of Science

by

Mahtab Shahkarami

December 2005

INFORMATION TO USERS

The quality of this reproduction is dependent upon the quality of the copy submitted. Broken or indistinct print, colored or poor quality illustrations and photographs, print bleed-through, substandard margins, and improper alignment can adversely affect reproduction.

In the unlikely event that the author did not send a complete manuscript and there are missing pages, these will be noted. Also, if unauthorized copyright material had to be removed, a note will indicate the deletion.

ProQuest Information and Learning Company
300 North Zeeb Road
P.O. Box 1346
Ann Arbor, MI 48106-1346

APPROVED FOR THE DEPARTMENT OF BIOLOGICAL SCIENCES

Dr. William Murray
San José State University

Dr. David Bieber
San José State University

Dr. Gary Schoolnik
Stanford University

APPROVED FOR THE UNIVERSITY

11/08/05

ABSTRACT

VIBRIO CHOLERAE BIOFILM DEVELOPMENT ON NATURAL AND ARTIFICIAL CHITIN SUBSTRATES

by Mahtab Shahkarami

Biofilm formation on chitinous substrates has been implicated in *Vibrio cholerae* survival in its natural aquatic habitats. Patterns of development and genetic requirements of *V. cholerae* O1 El Tor biofilms were investigated in seawater on (1) crab carapaces in a static system and (2) artificial chitin films in hydrodynamic systems (chemostat reactors and laminar flow cells). Adherent monolayers of isolated cells developed microcolonies and formed thick confluent layers of cells (mature biofilms) on both crab carapaces and artificial chitin. Mutants of *mshA* and *flaA*, but not *pilA*, exhibited reduced biofilm forming capacity on crab carapaces, suggesting that MSHA and flagellum play a role in early biofilm development. Mutants of the chitin sensor gene, *chiS*, were able to develop biofilm on artificial chitin, suggesting that a non-*chiS* mediated pathway exists for chitin utilization.

ACKNOWLEDGEMENTS

I gratefully acknowledge Dr. Gary Schoolnik (Stanford University School of Medicine) for kindly providing laboratory space, resources, and support necessary for this thesis research. I also gratefully acknowledge Michael Miller at the Schoolnik Laboratory for his invaluable expertise and assistance in the design, construction, microscopy, and analysis of chemostat and laminar flow cell experiments. I thank all the members of the Schoolnik Laboratory for their support and suggestions, Dr. David Bieber and Dr. William Murray for advising and critical reading, and Dr. Sulekha Anand for statistical analyses.

INTRODUCTION

Vibrio cholerae, the etiological agent of epidemic cholera, is a gram-negative, curved bacillus found in diverse aquatic habitats. It causes an acute and sometimes fatal disease in humans marked by watery diarrhea and fluid loss. *V. cholerae* has been isolated from marine, estuarine, and freshwater environments and is considered to be an indigenous constituent of these habitats. Members of the genus *Vibrio* are abundant and ubiquitous in the marine biosphere (13, 52). *V. cholerae* strains are categorized based on the somatic O-antigen; epidemic strains of *V. cholerae* belong to the O1 and O139 serogroups, and both serotypes produce an enterotoxin known as cholera toxin. The O1 serogroup, responsible for Asiatic cholera, has been further divided into two biotypes, classical and El Tor. While the classical biotype has been associated with the first six recorded pandemics of cholera, *V. cholerae* O1 El Tor is responsible for the current seventh pandemic and, currently, dominates cholera world-wide (59). In 1992, a new O139 strain emerged in India and Bangladesh, possibly beginning an eighth pandemic (40).

The presence of virulence genes in nontoxigenic *V. cholerae* suggests clonal origin of pathogenic strains from environmental strains (9, 18, 45). Sequencing studies have shown that sixth-pandemic, seventh-pandemic, and U.S. Gulf Coast isolates evolved from environmental, nontoxigenic, non-O1 strains by acquiring virulence genes (29). Pathogenicity of *V. cholerae* O1 and O139 requires the expression of three major virulence genes: cholera toxin, toxin co-regulated pilus (TCP) and the central regulatory protein, ToxR (51). These genes can be laterally exchanged between different strains

(44); virulent genes can be conferred to nontoxigenic strains by horizontal gene transfer in the environment or human gut (56). While non-O1 strains predominate aquatic habitats, *V. cholerae* O1 has been isolated from habitats thought to be independent of human input.

In its aquatic habitats, *V. cholerae* is found as a free-living bacterium or in association with aquatic life forms, such as zooplankton, phytoplankton, crustaceans, algae, insects, and plants (26-28, 43). *V. cholerae* O1, O139, and non-O1 strains produce chitinases and are capable of utilizing chitin as a carbon and nitrogen source (21). Evidence of *V. cholerae* attachment with chitinous invertebrates, as well as the ability to utilize nutrient sources outside the human host, point toward a natural aquatic niche of *V. cholerae* O1 (28, 48). The intermittent outbreaks of cholera in endemic areas of Bangladesh and India have correlated with seasonal blooms of zooplankton and phytoplankton to which *V. cholerae* attach (33). Numerous factors including climate changes, seasonal variability, and human input as well as the chemical, biotic, and abiotic composition of the aquatic reservoirs may affect the incidence and patterns of cholera transmission to humans (33).

V. cholerae undergoes an alteration of gene expression (phase variation), producing two colonial variants: smooth and rugose. On nonselective culture media, smooth variants produce smooth, translucent colonies while rugose variants produce wrinkled, opaque colonies. Smooth to rugose switching has been demonstrated to occur spontaneously under nutrient-limiting conditions (1, 62). Conditions inducing smooth to rugose switching and frequency of switching in *V. cholerae* O1 strains have also been

shown to vary by strain (1). The stability of the rugose phenotype has been speculated to vary by strain and the conditions regulating rugose to smooth reversion (1). Rugose morphology is marked by the production of copious amounts exopolysaccharide and has been linked to increased biofilm-forming capacity in *V. cholerae* O1 El Tor and non-O1 strains (62). Furthermore, rugosity has been shown to increase survival in chlorinated water and exposure to peroxide (36, 54). Genomic and expression analyses of smooth and rugose *V. cholerae* El Tor variants show that rugosity involves the synthesis of a *Vibrio*-specific polysaccharide (VPS) regulated by *vpsR* (61). Disruption of *vpsR* prevents the synthesis of VPS and confers smooth phenotype as well as atypical biofilm formation (61).

V. cholerae can adapt to changes in temperature, salinity, and nutrient availability (55) and can enter a dormant state, the viable but not culturable (VBNC) state, under unfavorable growth conditions (e.g., nutrient limitations or sub-optimal temperatures). The VBNC state in *V. cholerae* O1 and O139 is marked by the following characteristics: (1) the inability to grow on standard culture media; (2) changes in cellular morphology whereby cells decrease in size and change from comma-shaped to ovoid or coccoid forms; and (3) retention of membrane integrity and lower metabolic activity. *V. cholerae* O1 and O139 have also demonstrated to retain cholera toxin and toxin-associated genes in the chromosome for up to one year, thus remaining potentially pathogenic over extended periods of time (4, 8). The VBNC state may reflect survival strategies in response to unfavorable conditions and contribute to environmental persistence of pathogenic strains during inter-epidemic periods (4, 12).

Chitin adsorption and utilization. Adhesion to biotic and abiotic surfaces is likely an important adaptive strategy for *V. cholerae* survival in the environment. *V. cholerae* adsorbed onto chitin exoskeletons may persist for long amounts of time and be transported to more than one geographical location by currents and tides (11). *V. cholerae* adsorbed in crevices on zooplankton may also be protected from host defenses and survive digestion in mammals, allowing propagation and pathogenesis in the susceptible host. *V. cholerae* O1 El Tor adsorbed onto chitin particles, for example, survive in media acidified to the pH of human stomach better than non-adsorbed cells (37). Understanding biofilm formation on natural chitinous surfaces may provide insight into both the ecology and adaptive survival mechanisms of an environmental bacterium and human pathogen.

Chitin is a homopolymer composed of linear chains of β-(1,4)-linked N-acetylglucosamine (GlcNAc) residues cross-linked by hydrogen bonds. It is found in all kingdoms and stands as the most abundant natural polymer in the aquatic biosphere (63). Billions of tons of chitin are produced annually by copepods alone. The cuticles of molted and senescent copepods and other chitinous organisms continually fall to the ocean floor (referred to as "marine snow") and are degraded by chitinolytic bacteria (43). *Vibrios*, hence, play an important role in nutrient cycling by converting insoluble chitin into biologically useful forms of carbon and nitrogen.

Chitin utilization in *V. cholerae* is stringently regulated and estimated to involve dozens of enzymes and structural proteins, including those involved in chemosensory mechanisms (32). In general, chitin utilization by marine *Vibrios* begins with the sensing

and binding to chitin (63). Sensing of the chitin surface occurs by chemotaxis toward chemical gradients. The chemical gradients contain compounds released from natural decomposition or enzymatic degradation by polysaccharidases (chitinases) of chitinolytic bacteria. The chitin dimer, $(GlcNAc)_2$, serves as a potent attractant and may indicate nearby chitin availability since nearly all bacterial chitinases and most eukaryotic chitinases produce $(GlcNAc)_2$ as an end-product. Chemotaxis to chitin oligosaccharides has been extensively studied in *Vibrio furnissii*. Chitin mono- and oligo-saccharides, $(GlcNAc)_n$, n = 1–4, are chemoattractants for *V. furnissii* and are the most potent chemoattractants reported for bacteria (2, 30).

Chitin degradation follows two general steps in *V. cholerae*: (1) cleavage of the chitin polymer into chitin oligosaccharides by chitinases and (2) cleavage of chitin oligosaccharides to GlcNAc by chitobiases (47). After bacteria bind, secreted extracellular chitinases result in the release of GlcNAc, glucosamine, and oligosaccharides of GlcNAc and glucosamine (32). Chitin oligosaccharides pass through the outer membrane and enter the periplasmic space through a chitoporin, ChiP. $(GlcNAc)_2$ is sensed in the periplasmic space by a two-component chitin catabolic sensor, ChiS; ChiS and a chitin-binding protein are located on the inner membrane and, when modified by the presence of $(GlcNAc)_2$, induce the expression of chitinolytic genes (32). GlcNAc and $(GlcNAc)_2$ are transported by complexes in the inner membrane to the cytoplasm where they undergo enzymatic conversion to fructose-6-P, NH_3 and acetate.

Biofilm development. Gram-negative and gram-positive bacteria form specialized microbial communities (biofilms) on surfaces in the environment. The study

of biofilms has become of great interest in understanding the developmental pathways, antibiotic resistance, and ecology of aquatic bacteria (17). Formation of biofilm on nutritive surfaces helps maximize nutrient availability by increasing the number of cells fed by the nutrient source and by restricting the diffusion of mono- and oligo-saccharides away from the microenvironment. *V. cholerae*, *Pseudomonas aeruginosa*, and other gram-negative bacteria form biofilms in three developmental stages: (1) planktonic, when cells are free-swimming; (2) monolayer, when pioneering cells interact with and bind a surface in a transient manner, eventually binding permanently; and (3) mature biofilm, when cells form densely-packed layers and/or columns of cells surrounding water channels (58). Initial adhesion of bacteria to a surface by bacteria occurs by chance as a cell comes into contact with a surface (46) and is influenced by the physicochemical properties of the cell, surface, and surrounding medium (20). Chemical bonding, electrostatic, and van der Waals forces represent a few of the numerous attractive and repulsive forces present during adhesion (20, 22, 60). Further stability of nascent biofilm may be achieved through signaling systems activated by cell-surface contact. In *Escherichia coli*, for example, the Cpx signaling pathway is activated upon interaction with a hydrophobic surface and has been shown to regulate P-pili, perhaps enhancing surface adhesion (39). It is unknown if similar surface-sensing signaling pathways exist in other bacterial species.

Following initial adhesion to the surface and formation of a monolayer, bound pioneering cells form microcolonies of three to five cell layers deep. Microcolonies develop by clonal expansion and, perhaps, taxis of surface-associated or planktonic cells.

Reisner et al. have demonstrated that microcolony stability in *E. coli* depends on both clonal expansion and development (42). Furthermore, the proliferation of the pioneering cells may modify the surface composition and microenvironment, allowing for synergistic or competitive development of secondary cells (16). As the biofilm matures, cell density increases with the development of distinct architecture. Morphology of the mature biofilm varies with respect to the surface substrate, media conditions, and fluid shear stress (3). The depth of the mature biofilm in *V. cholerae* is regulated by quorum sensing mechanisms (64). At high *V. cholerae* cell density, accumulation of the auto-inducer, CAI-1, activates expression of HapR, which represses *vps* expression and promotes cell detachment from the biofilm (24, 35).

Attachment and colonization of chitin surfaces by *V. cholerae* O1 has been shown to require several surface proteins. More than one chitin binding protein (CBP) has been identified in several *Vibrio* species, including *V. cholerae* (49). The development of the initial monolayer on a non-nutritive glass surface by *V. cholerae* requires the regulation of mannose-sensitive hemagglutinin (MSHA) and flagellar motility. *V. cholerae* is highly motile by means of a single sheathed polar flagellum which may enhance initial attachment by generating the force necessary to overcome natural repulsive forces between the cell and surface. MSHA, a type IV pilus, mediates initial attachment and monolayer formation, independent of surface chemistry. On borosilicate glass, MSHA and flagellar motility accelerate attachment and monolayer formation by *V. cholerae* O1 El Tor (57, 58). MSHA has also been shown to mediate adherence to chitin; mutants that

do not express MSHA do not bind chitin beads as well as wild-type cells. Mutants lacking MSHA have also been shown to poorly colonize zooplankton (10).

A second type IV pilus, PilA, may have a potential role in attachment and colonization of chitin surfaces by *V. cholerae* O1 El Tor. Expression profiles of *V. cholerae* O1 El Tor exposed to chitin oligosaccharides and crab carapaces indicate up-regulation of *pilA* in the presence of chitin (34). Expression analyses also suggest that chitin-utilization and *pilA* gene products are polarly located in the cell body, further suggesting that PilA forms a specialized chitin-regulated-pilus, ChiRP (34). The function of ChiRP in *V. cholerae* remains unclear; Meibom et al. have proposed a potential role for ChiRP in mediating initial attachment to a chitin surface where pilus attachment and retraction orient the cell body for optimal chitin utilization (34). A recent study has demonstrated that a third type IV pilus, the toxin co-regulated pilus (TCP) also mediates biofilm formation on chitin. The function of TCP has been extensively studied and is considered as the primary adherence factor in intestinal attachment (50). TCP appears to be mediate microcolony formation on squid pen (a natural chitinous surface). There has been no evidence in a role for TCP in initial monolayer development, and thus TCP may not have a function in adhesion (41).

Adherence to and biofilm formation on chitinous surfaces, thus, is a noteworthy aspect of the ecology and epidemiology of *V. cholerae*. Crab exoskeletons, in particular, serve as a convenient substrate for studying *V. cholerae* attachment and colonization of chitinous organisms. *Vibrios* and other marine chitinolytic bacteria have been implicated in crab shell diseases (15, 53) Furthermore, edible crabs have been associated with

outbreaks of cholera in the United States and Peru (5, 19, 23). A previous study quantifying *V. cholerae* colonization of crab shells showed that *V. cholerae* O1 can attach and multiply on the crab shell surfaces (7).

This thesis describes the investigation of the developmental processes, genetic requirements, and patterns of biofilm formation on chitinous surfaces by *V. cholerae*. We employed three methods for biofilm culture on chitin substrates: (1) growth on natural chitin substrate (crab carapace) under static conditions; (2) growth on an artificial chitin substrate under chemostatic flow conditions; (3) growth on an artificial chitin substrate under laminar flow conditions. We used crab carapaces as a model for *V. cholerae* colonization on a natural chitinous substrate and visualized biofilm development by scanning electron microscopy (SEM). To mimic natural conditions of hydrodynamic flow and constant chemical stability in the surrounding media, we employed chemostatic reactors and laminar flow cells using a defined seawater medium and artificial chitin substrate, which allowed us to visualize chitin-specific biofilm development by confocal scanning laser microscopy (CSLM).

MATERIALS AND METHODS

Media and Growth Conditions. Luria-Bertani broth (LB) and LB agar were used as general-purpose growth media. Bacterial stocks were maintained in glycerol and LB (30% and 70%, respectively) at −80°C. Thiosulfate citrate bile salts agar containing gentamicin (5 mg/ml) (TCBS-gent) was used for selection of *V. cholerae gfp*-labeled mutants. A commercial artificial seawater diluted 1:2 (ASW) was used in crab carapace experiments. A defined seawater medium (468 mM NaCl, 55 mM $MgSO_4$, 3 mM $NaHCO_3$, 9.9 mM $CaCl_2 \cdot H_2O$), 10.3 mM KCl, 0.14 $Na_2B4O_7 \cdot 10H_2O$, 0.1 mM $SrCl \cdot 6H_2O$, 0.03 mM NaBr, 0.002 mM NaI, 0.026 mM LiCl) was used to make supplemented defined artificial seawater (SDASW) [50% defined seawater medium, 0.187 mM NH_4Cl, 18.7 mM K_2HPO_4, and 0.1× MEM vitamin mixture (Gibco)]. The following carbon and nitrogen sources were used: N-acetylglucosamine (GlcNAc) (Sigma), chitobiose [$(GlcNAc)_2$] (Seikagaku America), lactate, and casamino acids. SDASW containing 2.0% GlcNAc was buffered with 50 mM HEPES for batch cultures. M9 broth (Fluka, Switzerland), pH 7.4, was supplemented with 1.0 mM $MgSO_4$, 0.1 mM $CaCl_2$, and 0.1× MEM vitamin mixture. M9-chitin plates (M9-chitin) were made with 0.5% lactate and 0.5% chitin from purified shrimp shells (Sigma). Phosphate-buffered saline (PBS) was also used. All batch cultures were grown at 30°C with shaking; all plates were incubated at 30–37°C.

Bacterial strains and plasmids. The bacterial strains and plasmids used in this study are listed in Table 1.

Construction of *gfp*-labeled mutants. Triparental matings of *Escherichia coli* SM10, *E. coli* S17-1 and recipient *V. cholerae* strains were carried out on LB agar. Transconjugant *V. cholerae* clones were selected on TCBS-gent, screened for production of green fluorescent protein (GFP) and confirmed for chromosomal insertion of Tn7-GFP by PCR.

PCR. PCR Supermix (Invitrogen) was used for all PCR. PCR methods and primers for confirmation of *gfp* insertion were obtained from Michael Miller (Stanford University, Stanford, CA). The following primers were designed for PCR amplification of *chiS* gene (VC0622) fragments: (1) 5'–TGATGCACGGCACTCTCTAC–3' and 5'–ACGCGCGATGTTTCAACTCTT–3' (flanked a 611 bp fragment within VC0622) and (2) 5'–GCTCTAGACGCTTTAGCTTGGACTTA–3' and 5'–GCGAGCTCTTGCAATTTATCGCTGC–3' (flanked an approximately 3500 bp fragment including VC0622). DNA products were visualized by agarose gel electrophoresis.

Crab carapace timecourse assay. Dorsal crab carapaces from *Cancer magister* were cut into approximately 10 mm^2 pieces, autoclaved, and placed in flat-bottomed tissue culture plate wells. *V. cholerae* strains were cultured overnight in M9 broth containing 0.5% lactate, washed, and diluted 1:25 in ASW to make inoculum. Crab carapaces were rinsed and transferred to wells containing fresh ASW after 24 hours of static incubation with 1.0 ml of inoculum at room temperature. Crab carapaces continued static incubation at room temperature for remainder of timecourse and were sampled every 24 hours for scanning electron microscopy.

Scanning electron microscopy of crab carapaces. Crab carapaces were gently rinsed four times in ASW, fixed in 2% glutaraldehyde in 0.1 M sodium cacodylate buffer, pH 7.4 for 30 minutes at room temperature and stored at 4°C until further processing. The fixed specimens were rinsed three times in 0.1 M sodium cacodylate buffer, post-fixed in 1% OsO_4 at room temperature for one hour, rinsed five times with deionized water, and dehydrated with increasing concentrations of ethanol (50, 70, 80, 95, and 100%) for 10 minutes each. The specimens were critical point dried using bone-dry CO_2, mounted onto aluminum stubs using carbon adhesive, and coated with gold and palladium (60:40, respectively) in a Pelco SC-7 Auto Sputter Coater (Ted Pella Inc.). Specimens were viewed in a Philips XL40 scanning electron microscope (FEI Co.) with an accelerating voltage of 10 kV, spot size of 2–5 μm, and working distance of 10 mm (approximately). Images were stored on zip disks in tagged image file format (TIFF) and copied to a computer hard drive and compact disks for permanent storage and further image analysis using Adobe Photoshop 7.0 software (Adobe Systems Inc.). Specimens were stored in a desiccating cabinet at room temperature.

Statistical analyses of crab carapaces. SEM micrographs taken at 2000× magnification were quantified for (1) the establishment of a monolayer and (2) formation of microcolonies. Micrographs were visually scored for the establishment of monolayers by the presence of ≥ 200 cells in a field. The number of micrographs meeting the criterion of ≥ 200 cells in a field was divided by the total number of micrographs to give percentage of micrographs displaying an established monolayer. Micrographs were visually scored for microcolony development by the presence of ≥ 1 microcolony of ≥ 10

cells in a field. The number of micrographs meeting the criterion of ≥ 1 microcolony of ≥ 10 cells in a field was divided by the total number of micrographs to give percentage of micrographs displaying microcolony development. Percentages were analyzed and tested using the Chi-squared test of significance. Statistical testing and analyses were performed by Dr. Sulekha Anand (San José State University, San Jose, CA).

Preparation of chemostat reactors. A diagram of a chemostat system is shown in Figure 1. For each experiment, a series of chemostat reactors (chemostats) were made from 50-ml conical polypropylene centrifuge tubes. Each chemostat was topped with a rubber stopper containing two needles, one for media inflow, which delivered media to the top of the reservoir, and another for air inflow, which was delivered by a tube extending into the bottom of the reservoir. Media was pumped from media reservoirs by a Watson-Marlow 250U peristaltic pump (Watson-Marlow Bredel Inc.) through silicone tubing to the chemostats. Air was delivered by a Tetratec 150 air pump (Tetra U.S.) through silicone tubing, passing through a 0.45 μm syringe filter, to the chemostats. Chemostat effluent exited an outlet hole near the reservoir fill-line and was deposited into a media waste container placed below the level of the chemostats. Chemostats, artificial chitin mounts, and relevant tubing were flushed with reagent-grade water and autoclaved prior to the start of media flow.

Preparation of artificial chitin mounts for chemostats. Thin artificial chitin films obtained from Eugene Khor (National University of Singapore, Singapore) were used as the solid substrate and nutritional source for *V. cholerae* colonization and growth. Translucent silicone rubber adhesive (General Electric) was applied to one side of the

chitin film to produce a solid support approximately 3 mm high. Chitin films and adhesive were cured for 48–72 hours in a fume hood and cut into 10 mm^2 pieces to make chitin mounts. Chitin mounts and 12 mm diameter round glass coverslips were affixed to glass slides (7.6 by 2.5 cm) using silicone adhesive, cured for 24–48 hours, and autoclaved.

Inoculation of chitin mounts and timecourse experiments in chemostats. The *gfp*-labeled *V. cholerae* strains were grown in SDASW containing 2.0% GlcNAc or as indicated, washed, and diluted to an optical density of 0.2 at 600 nm (OD_{600} = 0.2) in SDASW containing 0.01% $(GlcNAc)_2$ or as indicated to make inoculum. After static incubation with inoculum (40 ml per slide) at 30°C for six hours or as indicated, slides were gently rinsed in 30°C SDASW to remove unattached cells, immediately placed in chemostats containing media, and incubated at 30°C with a flow rate of 500 ml/hr.

Sampling of chemostats during timecourse. Chitin, glass mounts, and planktonic cells were sampled from chemostats every 24 hours. Mounts were removed from the same position at each timepoint across chemostats for sampling consistency, beginning from the bottom row at the first timepoint. For microscopy, mounts were fixed by incubating in a modified paraformaldehyde phosphate buffer, pH 7.4, for one hour away from light (to prevent photobleaching). The fixed mounts were rinsed two times in PBS and then attached to the bottom of a Petri dish with silicone adhesive, covered with PBS, and stored in the dark at 4°C until viewing. Planktonic cells were sampled from chemostat reservoirs prior to sampling of mounts and biofilm-associated cells were

sampled by scraping cells on chitin surface with a pipet tip and resuspended with 1 ml PBS; cells were serially diluted and plated on LB agar for enumeration.

Confocal scanning laser microscopy (CSLM) of chitin surface in chemostats experiments. Chitin and glass surfaces were viewed by CSLM on a Carl Zeiss Laser Scanning System (LSM-510) (Carl Zeiss Microimaging). Two representative z-stacks were scanned at surface level using a 40× water immersion objective. Scanning was conducted by a 488-nm Argon laser with a bandpass filter set at 500–530 nm for GFP fluorescence and a 543 nm HeNe laser with a longpass filter set at 560 nm for chitin fluorescence. Images were stored onto compact disks for further analysis with Imaris 4.1.3 software (Bitplane AG, Switzerland).

Preparation of laminar flow cells. Laminar flow cells (Biosurface Technologies Corp.) were constructed with 28 by 5 by 2 mm chambers (Fig. 2). Artificial chitin films were affixed to plastic coupons with a thin layer of silicone adhesive and placed in the chamber bottom. A glass coverslip, No. 0 thickness (24 by 60 mm) (Ted Pella Inc.) or No. 1 thickness (24 by 50 mm) (VWR Scientific), sealed with silicone adhesive, covered the chamber top. Media was pumped by a Watson-Marlow 250U peristaltic pump through silicone tubing, interrupted by gas traps, and delivered to flow chambers. Media effluent exited through silicone tubing at an elevation 10–15 cm higher than the level of the flow cells and gas traps to reduce back pressure and bubbles in flow chambers. Flow cells containing chitin were decontaminated in 95% ethanol for 5–18 hours, aseptically connected to autoclaved tubing, flushed with sterile reagent-grade water for 3–18 hours, then flushed with media for 2–4 hours at 30°C prior to seeding.

Seeding of flow chambers and timecourse experiment in laminar flow cells. Overnight cultures of *gfp*-labeled N16961 were grown in M9 containing 2% GlcNAc, diluted 1:1000 in fresh media, grown to mid-exponential phase (OD_{600} = 0.2), then washed and resuspended in M9 containing 0.01% $(GlcNAc)_2$ to make inoculum. Each chamber was seeded, glass-side up, with 1 ml inoculum by injection and incubated for one hour under static conditions. Flowrate was set to 20 ml/hr for timecourse. M9 containing 0.001% $(GlcNAc)_2$ was used for the first 24 hours of timecourse, M9 alone was used for remainder of timecourse.

Confocal scanning laser microscopy (CSLM) of laminar flow cells and image analysis. Surface-associated cells on both the chitin and glass were viewed by CSLM and phase contrast microscopy at 1-, 24-, and 48-hour timepoints using the same scanning parameters, data storage, and image analysis methods as described above for chemostat experiments. Two representative z-stacks of chitin and glass surfaces near the center of the chambers were scanned.

Scanning electron microscopy of chitin surface in laminar flow cells. N16961 biofilm cultured in timecourse experiment was allowed to incubate for an additional 24 hours in M9 alone (72 hours of total incubation). Flow was stopped and 1 ml of 2% glutaraldehyde in 0.2 M Sorenson's sodium phosphate buffer, pH 7.4, was slowly injected into the chamber and allowed to incubate for 30 minutes at room temperature. Chambers were gently rinsed three times with 0.2 M Sorenson's sodium phosphate buffer, pH 7.4, by injection. Glass coverslips and chitin mounts were removed and post-fixed in 1% OsO_4 at room temperature for one hour, rinsed five times with deionized

water, and dehydrated with increasing concentrations of ethanol (50, 70, 80, 95, and 100%) for 10 minutes each. The specimens were critical point dried, mounted, sputtercoated and viewed as described above for crab carapace preparation.

RESULTS

Biofilm development on crab carapace. We visualized *V. cholerae* adhesion on a chitin surface and tested the role of *pilA* and *mshA* in the developmental process of biofilm formation using scanning electron microscopy (SEM). The crab carapace served as a natural chitin surface and substrate, previously shown to harbor surface-associated *V. cholerae* (6, 7). The intermolt crab exoskeleton consists of an thin outer epicuticle and three layers of a procuticle (exocuticle, endocuticle, and membranous layer) (14, 31, 38). The epicuticle consists of proteins, lipids and calcium salts, and does not contain chitin; it is impermeable to prevent loss of water and solubilization of exoskeletal components (38). SEM of the crab carapace revealed heterogeneous architecture on both topside and underside surfaces (Fig. 3). The topside is comprised of smooth areas of intact epicuticle, spikes and damaged areas containing crevices and shallow pits exposing the underlying procuticle (Fig. 3A). The procuticle consists of a chitin-protein composite that is calcified (mainly with calcite); the innermost membranous layer, however, is not calcified (38). SEM of the underside revealed rough and rippled surfaces, mostly homogeneous in a large field of view (Fig. 3B). In some specimens, cracks in the form of striations were present, spanning most or the entire surface in the field of view, as seen below in N16961Δ*pilA* micrographs (Fig. 4, Plate 2). Pore canals (50–250 μm diameter) were distributed (0.1–1.0 mm apart) throughout the underside (data not shown).

Figure 4 shows the development of N16961, N16961Δ*pilA* (Δ*pilA*) and N16961Δ*mshA* (Δ*mshA*) biofilm on the topside of crab carapaces. Representative areas containing both intact and damaged surfaces, if present, were selected for comparison.

All strains tested (N16961, Δ*pilA* and Δ*mshA*) showed evenly distributed isolated cells after one day of incubation. Cell densities of N16961 and Δ*pilA* were similar to and greater than those of Δ*mshA*. N16961 and Δ*pilA* persisted on the surface and increased in density over time. Monolayers, multiple cell layers and clumps of cells were more common in damaged areas than areas of intact epicuticle, suggesting that cells may not be able to adhere well or have the enzymes necessary to penetrate the surface.

Extracellular material production in the form of non-flagellar web-like material associated with the cell body was present on isolated and aggregated cells, and was present in all areas of growth by day 4 (Fig. 4, Plate 2). This extracellular material may be VPS, produced as cells adherently proliferate on the surface. Isolated Δ*mshA* cells also persisted but did not proliferate as well as N16961, with relatively few and small clumps forming in the damaged areas (almost none in intact areas) as the other strains. All strains exhibited polar flagella throughout the timecourse. Non-flagellated mutant, Δ*flaA*, failed to form a monolayer and/or clumps, with only five or fewer isolated cells observed on the carapace surface in each specimen at days 1, 2, and 4 (data not shown).

Figure 5 shows the development of N16961, Δ*pilA* and Δ*mshA* biofilm on the underside of crab carapaces. After day 1 of incubation, N16961 and Δ*pilA* formed evenly distributed monolayers of similar densities while Δ*mshA* formed a relatively sparse monolayer. Monolayers of all strains increased in density over time and displayed biphasic patterns of biofilm development that consisted of isolated cells distributed evenly between microcolonies. N16961 and Δ*pilA* biofilms had shifted from biphasic growth patterns to confluent growth at day 3 and 4. Monolayers of Δ*mshA* developed

similar biphasic growth patterns shifting towards homogeneous and confluent growth, but at a slower rate than the other strains. At day 4, Δ*mshA* formed varying patterns of biofilm, producing monolayers of predominantly isolated cells, biphasic monolayers, and multi-layered confluent growth similar to N16961 at the same timepoint.

On surfaces containing striated cracks, all strains had partially or completely penetrated underneath the uppermost layers, suggesting that the cells had burrowed through the substrata. It is unknown whether the absence of cells on the uppermost layer is due to non-utilizable substrate or the removal of cells during rinsing and processing. The variances in surface architecture and flaking of the surface in later timepoints after critical point drying suggested possible sloughing of dense cell biomass after sampling. Populations of cells observed from later timepoints, hence, may be remnants of a thicker biofilm that had detached from shearing stress. Polar flagella persisted throughout the timecourse and were often seen tangled with other cells and flagella in cell aggregates.

The timecourse of biofilm development by non-flagellated mutant, N16961Δ*flaA* (Δ*flaA*), is shown in Figure 6. Like N16961, Δ*flaA* produced a monolayer in the first day of incubation. Isolated Δ*flaA* cells, however, failed to form microcolonies and increase in overall cell density as N16961 in the later timepoints, persisting as isolated cells throughout the timecourse. The failure of Δ*flaA* to form comparable cell layers and microcolonies to wild-type on both the topside and underside suggests that the flagellum is necessary for microcolony formation and proliferation, and perhaps recruitment of isolated cells to the microcolony. The presence of isolated Δ*flaA* cells on the surface, however, suggests that the flagellum is not required for binding to the surface. The

distribution of isolated Δ*flaA* cells is likely due to gravity whereby non-motile cells make contact with the surface below by sinking in the medium rather than sensing of and taxis to the surface.

Patterns of attachment during intermediate stages of biofilm development on crab carapace. To assess the role of PilA and MSHA in forming the monolayer, we examined the patterns of isolated cell and microcolony distribution prior to formation of dense biomass. We did not know what phenotype to expect from PilA; previous findings suggesting ChiRP involvement in early colonization lead us to expect differences in isolated cell attachment morphology and overall cell density during early monolayer development. We also expected to see poor colonization by Δ*mshA* and a decreased ability to form a monolayer comparable to wild-type as observed in our previous SEM studies. Due to the problems with the topside crab carapace surface (heterogeneous topography and impermeable epicuticle), we chose to quantify attachment to the underside substrate.

Crab carapaces were quantitatively assessed for the presence of bound cells and microcolonies after 48 hours of incubation. We faced several problems in quantifying total cell numbers and microcolonies for the following reasons: (1) uneven cell distribution as a result of surface heterogeneity; (2) inability to enumerate cells in microcolonies without dispersing the clumps of cells; and (3) presence of cryptic cells partially or completely hidden from view. Instead of directly quantifying cell numbers, we visually scored the images for the presence of a monolayer and microcolony development based on simple criteria (Refer to Materials and Methods, Statistical

analyses of crab carapaces). Figure 7 clearly indicates that there is no significant difference between N16961 and Δ*pilA* in monolayer and microcolony formation ($P > 0.05$). Results from this and timecourse assays show no obvious role for PilA in attachment/microcolony development and proliferation. MSHA mutants, however, did not bind as well as wild-type (indicated by presence of < 200 cells) and were only present as isolated cells (no microcolonies formed) (Fig.7, $P > 0.05$). Poor monolayer formation by Δ*mshA* is likely due to weak adhesion as Δ*mshA* was able to form a delayed but comparable biofilm relative to wild-type during later timepoints in the previous experiments. MSHA, hence, is required for adhesion to the surface in early monolayer formation but is not required for overall biofilm development.

Confocal scanning laser microscopy (CSLM) of *V. cholerae* biofilm development on artificial chitin under chemostatic flow conditions. We investigated *V. cholerae* biofilm development on chitin under chemostatic flow conditions. Chemostats were used to mimic natural conditions for biofilm growth by providing continual exchange and movement of media over an attachment substrate, probably reducing rates of reattachment by planktonic cells, and reducing the accumulation of waste products. In order to overcome problems with surface heterogeneity within biotic chitin substrates, we used artificial chitin films as the attachment and nutrient substrate. A previous SEM study of a *V. cholerae* O1 El Tor A1552 biofilm on artificial chitin demonstrated biomass similar to that seen in our SEM studies of N16961 on crab carapaces, as well as a smooth surface of the artificial chitin film itself (data not shown). Furthermore, the artificial chitin was chemically defined, synthesized from purified chitin

devoid of contaminating proteins and $CaCO_3$. To visualize cells by CSLM, we used *gfp*-labeled *V. cholerae* strains constructed to constitutively express GFP.

Monolayers of N16961 on artificial chitin were incubated in chemostats in a timecourse assay (Fig. 8). Cell density of the monolayers increased and developed in a biphasic manner, with areas of isolated cells (as observed after inoculation) and microcolony formation. Isolated cell density decreased during the first day while numbers of small microcolonies increased. Microcolonies formed as symmetrical and dense aggregates of cells penetrating the chitin surface as distinct structures (pitting). Pitting was observed at all subsequent timepoints. At day 2, the density of isolated cells and microcolonies and microcolony size had increased in surface coverage. The biphasic nature of growth shifted to more homogeneous patterns of growth, consisting of less localized and more confluent growth over the entire field by day 3. At this point, the surface was covered by a dense layer of cells with the exception of gaps (red fluorescence). The gaps varied in shape and were elevated above the chitin level, suggesting that they are non-utilizable pieces of artificial chitin membrane. At day 4, a dense biofilm of multiple cell layers and flat surface had developed along with pitting. At day 5, the biofilms displayed sloughing (seen as flaking during sampling and detached biomass by phase contrast microscopy) likely due to shearing stress, aging biofilm and/or destabilization of chitin substrate. CSLM revealed thin layers of attached cells remaining on an uneven chitin surface at day 5.

Role of ChiS in biofilm development on artificial chitin in chemostats. To clarify the initial events of chitin colonization, we investigated the role of ChiS, a hybrid

sensor kinase of the Arc B type located in the inner membrane, encoded by *chiS*. ChiS has been previously implemented in the control of chitin catabolic cascade genes through sensing of $(GlcNAc)_n$ ($n > 1$) (32). We tested VCXB21 (wild-type) and a *chiS* deletion strain, VCXB21Δ*chiS* (Δ*chiS*), in a timecourse experiment. In order to rule out the presence of non-chitin nutrient sources in the chemostats, we also tested a double chitinase-deficient mutant, Δ*chiA-1A-2*, previously shown to be incapable of utilizing chitin as a nutrient source (34), as a negative control. All strains formed typical monolayers after the initial binding step. Monolayers of Δ*chiA-1A*-2 persisted continuously with no observable microcolony development. Initial monolayers of N16961 (data not shown) and VCXB21 increased in isolated cell and microcolony density, leading to thick biofilm production and sloughing by 5 days (Fig. 9). Initial Δ*chiS* monolayers persisted without noticeable changes to density and morphology for the first 3 days. By day 4, however, microcolonies had developed; microcolony and isolated cell density increased for the duration of the timecourse experiment, resulting in thick biofilm covering the entire field by 6 days (Fig. 9).

To confirm chitin utilization by Δ*chiS* and select isolates for further tests, we plated day 5 biofilm-associated cells (VCXB21, Δ*chiS*, N16961 and Δ*chiA-1A-2*) for chitin-clearing on M9-chitin agar and quantification of rugosity on LB agar. All isolates displayed clearing on M9-chitin agar, indicated by clear zones around a colony (Fig. 10). Colony size and zones of clearing by Δ*chiA-1A-2* were smaller than wild-type, suggesting that at least a third chitinase is produced by N16961 and that the additional chitinase(s) are produced in lesser quantities than the sum of chitinases produced by *chiA-1* and *chiA-*

2. Clearing on M9-chitin agar by Δ*chiS* was indistinguishable from wild-type, suggesting that chitin catabolic genes, including chitinases, were equally induced.

We measured rugosity within the planktonic and biofilm-associated cell populations by the percentage of CFU displaying rugose morphology. Rugosity within the planktonic cell population at day 3 was dramatically higher among wild-type strains than mutant strains (96.6% N16961; 96.6% VCXB21; 1.6% Δ*chiA-1A*-2; and 3.9% Δ*chiS* rugose CFU) (Fig. 11). Biofilm-associated cells harvested at day 5 also demonstrated higher percentages of rugose CFU in wild-type strains than mutant strains (100.0% N16961; 97.9% VCXB21; 3.4% Δ*chiA-1A-2*; and 0.0% Δ*chiS* rugose CFU). Growth of wild-type and Δ*chiS* strains on artificial chitin, thus, induced switching from smooth to rugose colony morphology. However, the switch was more prominent in the wild-type strains, perhaps due to increased nutrient availability and the increases in biomass and differentiation within the biofilm communities. Higher percentages of rugose morphotypes in the wild-type biofilms suggest that rugosity is involved in community survival on chitin.

To test whether chitin catabolism is induced by the experimental treatments in Δ*chiS*, we plated the experimental isolates and stock cultures, which had not been exposed to chitin, on M9-chitin agar. All experimental and stock isolates of Δ*chiS* displayed chitin clearing (Fig. 12). Chitin-clearing by Δ*chiS* suggests that a non-ChiS regulated pathway exists in sensing chitin and inducing the chitin catabolic cascade.

Effects of $(GlcNAc)_2$ on biofilm development on artificial chitin in chemostats. In the microenvironment of chitin-degrading bacteria, the main product of

chitin degradation, $(GlcNAc)_2$, is present and serves as a both utilizable nutrient and signal for chitin utilization. To assess the effects of $(GlcNAc)_2$ on the development of *V. cholerae* biofilms, we prepared monolayers of N16961 on artificial chitin and supplemented the chemostat media with 0.001% $(GlcNAc)_2$ during the first 12 or 24 hours (12-hour and 24-hour treatments, respectively). The initial monolayers were prepared in a similar manner as in previous experiments with the following exceptions: (1) Overnight cultures of N16961 were grown nutrient-rich media (LB broth); (2) inoculum was prepared with SDASW containing 0.001% $(GlcNAc)_2$; and (3) chitin and inocula were incubated for one hour in the binding step (refer to Materials and Methods, Inoculation of chitin mounts and timecourse experiments in chemostats). For all treatments, monolayers developed biphasic growth patterns as described above, with isolated cell densities decreasing in the first day while the frequency of microcolonies increased (Fig. 13). During this period, control treatments, which were not exposed to supplemental $(GlcNAc)_2$ in the chemostats, underwent the largest loss of isolated cells, exhibiting sparsely distributed isolated cells and microcolonies by day 1. This monolayer morphology persisted for 3 days, after which time a biofilm several cells thick had developed with pitting. Biofilms grew at a faster rate with consistent patterns of biphasic development within $(GlcNAc)_2$ treatments. Development in the 24-hour treatment was faster than the 12-hour treatment in the appearance and proliferation of microcolonies.

CSLM of *V. cholerae* biofilm development on artificial chitin films under laminar flow conditions. We further investigated biofilm development under hydrodynamic flow conditions using laminar flow cells, which allowed us to visualize

living biofilms. Laminar flow chambers containing artificial chitin films and glass were used to grow biofilms under constant, unidirectional flow conditions. Live biofilm in flow chambers seeded with *gfp*-labeled N16961 was viewed by CSLM and phase contrast microscopy at 1-, 24- and 48-hour timepoints. During the timecourse, biomass was generally concentrated toward the edges of the channels, indicating variations in growth conditions within the chamber, possibly due to chamber geometry and air pockets altering flow dynamics. We selected locations at the center of the chamber for image acquisition, selecting for areas under consistent flow conditions. Due to inadequate resolution in the z-axis, we were unable to determine the extent of pitting by microcolonies.

Representative images of biofilm development on chitin and glass are shown in Figure 14. One hour after the onset of flow, planktonic cells migrated downstream while monolayers remained attached to chitin and glass. Monolayers on chitin and glass developed small clusters by 24 hours. Monolayers on the glass surface varied in density relative to monolayers on chitin, with either less or comparable biomass on glass. Variability on the glass may have been due to residual nutrients left on the glass from handling, flow cell preparation, and/or passage of air bubbles through the flow chamber. During this initial period of incubation (1–24 hours), surface-associated cells exhibited the following behavior: immobilized, twitching in situ, spinning in circles (likely anchored by flagellum) and darting. Furthermore, gross swarming did not occur, taking place only when media flow was restricted. By 48 hours, after 24 hours of M9 alone, all chambers exhibited dense biomass throughout the chitin surface with shallow pitting.

Biphasic monolayer development similar to that observed in chemostat experiments took place within the first 24 hours. Initial monolayers developed with increasing numbers of microcolonies and isolated cells. Biomass on the glass was reduced and cells exhibited relatively dim fluorescence, altered cell morphology (increased frequency of isolated coccoid cells) and no movement. Growth in M9 alone, thus, was directed to the chitin surface, indicating chitin-specific biofilm development. Furthermore, filamentous corkscrew-shaped cells were observed during the timecourse as isolated cells on chitin/glass substrata, fluorescing green with similar intensity as typical cells (data not shown). Clumps of filamentous cells were also observed on chitin (data not shown), suggesting clonal expansion of this morphotype.

To visualize the chitin surface in closer detail than CSLM, we performed SEM of a 72-hour biofilm which had reached maturation and may have undergone sloughing. The chitin surface was intact toward the center of the chamber and was relatively thinner at the edges, evident by the exposed substratum (silicone adhesive) at the edges. Decomposition of the substratum, hence, may have contributed to the sloughing of biomass at this stage of development. Figure 15 shows micrographs of the sloughed surface with remaining attached cells. The cells are similar to the typical curve-shaped cells often observed in the micrographs of the crab carapace experiments. The longer corkscrew-shaped (filamentous) cells that were less often observed in the crab carapace experiments were also present in the sloughed biofilm. The filamentous cells displayed similar cell body widths and a single polar flagellum as typical cells. These

morphological characteristics in addition to green fluorescence (observed by CSLM) suggest that the filamentous cells are likely *V. cholerae* rather than a contaminant.

DISCUSSION

This is the first study to investigate and visualize *V. cholerae* O1 El Tor biofilm development on a biotic chitin surface, the crab carapace, in defined seawater medium using SEM. Biofilm development by *V. cholerae* O1 and O139 has been previously demonstrated on borosilicate glass in LB broth and carbon-supplemented seawater (57, 58) and on squid pen in mineral medium (41) under similar static conditions. In this investigation, crab carapaces served as the sole carbon, nitrogen and energy source, as well as an attachment substrate, similar to conditions encountered in the marine environment where soluble nutrients are scarce. We found crab carapaces as a good model for studying the colonization of a natural chitin substrate for the following reasons: (i) the carapace underside is colonizable by N16961, as shown by the confluent growth of biofilm spanning entire fields of view (Fig. 5, Plate 2); (ii) the surfaces are relatively flat, denser than seawater, and polarity of the carapace (topside and underside) is easily identified; and (iii) the carapaces are easily obtained, prepared and processed for SEM. As mentioned previously, the natural and unknown variations in surface architecture and chemical composition of the crab carapaces lead to imprecise quantification of cell numbers and distribution. Other drawbacks of this system include the inability to provide a chemically static environment and accumulation of waste products and diffused nutrients in the media. Future experiments with crab carapaces may be adapted to chemostat reactors to create more favorable culture conditions.

In a previous study of PilA, Meibom et al. hypothesized a role for PilA as a subunit of ChiRP, which may orient the cell body at the flagellar end as to enhance chitin

utilization (34). We hypothesized that, when *V. cholerae* is exposed to the crab carapace, ChiRP is synthesized and functions to orient the cell body perpendicularly to the surface during early monolayer development. This study, however, revealed no observable differences between wild type cells and mutants lacking PilA. PilA also did not affect morphology of cell-surface and cell-cell adhesion structures formed during biofilm development. Of course, the experimental procedures may have prevented visualization of the hypothetical cell body orientation during initial adhesion of cells to the surface. The duration of pilus formation, adhesion and retraction may occur in a relatively short amount of time and may be overlooked during the initial 24-hour binding period. Our processing procedures may have also caused polarly-adhered cells to detach and laterally-adhered cells to remain. Future studies identifying and locating ChiRP on the cell body may allow direct visualization of pilus formation, if present, during initial adhesion and monolayer development.

Our investigation of the role of MSHA in *V. cholerae* monolayer formation and biofilm development on the crab carapace is consistent with previous studies of *mshA* mutants on borosilicate glass (57, 58) and zooplankton (10). The absence of MSHA lead to dramatically less adhesion of cells to the carapace; cells may have not adhered or may have been weakly adhered prior to rinsing (prior to timecourse and during preparation for SEM). The lag in biofilm development by Δ*mshA*, thus, was likely due to a smaller population of retained cells rather than a decreased ability to utilize chitin. Indeed, MSHA may have a greater role in conditions of hydrodynamic flow where cells must overcome numerous forces against binding.

The role of the flagellum in monolayer formation and biofilm development on the crab carapace remains unclear. A previous study has shown that flagellar motility is necessary for *V. cholerae* O1 El Tor to form biofilm at the same rate as wild-type on borosilicate glass (58). Furthermore, there was no difference in the rate of biofilm formation by mutants lacking a flagellum and mutants with a paralyzed flagellum on borosilicate glass (58). Future studies of Δ*flaA* on crab carapaces should include longer timepoints to capture further biofilm development (which may occur at a slower rate than N16961). Comparison of Δ*flaA* to a mutant with an intact but paralyzed flagellum may also elucidate the mechanism by which flagellar motility mediates biofilm development. The absence of flagellar subunits in a non-flagellated mutant may alter the structure or function of other membrane-associated complexes, possibly affecting signaling and chitin utilization pathways.

This is also the first study to investigate *V. cholerae* O1 El Tor biofilm development on an artificial chitin substrate in a defined seawater medium under hydrodynamic flow conditions using CSLM (3). Laminar flow cells have been previously used in a study of biofilm development by *Pseudoalteromonas* on chitin film-coated coupons and squid pen by CSLM. The study also found squid pen to be an unsuitable substrate due to surface roughness and autofluorescence (3). Both our chemostat and laminar flow cell systems were designed to mimic natural conditions in the marine environment by preventing the accumulation of waste products (i.e., establishing a chemically static environment) and exposing the cells/biomass to fluid shear stress. Reduction in the incidence of reattachment by detached and planktonic cells,

however, was arbitrary; reattachment may occur under natural conditions. The extent of reattachment in either of our flow systems is unknown and remains as an insurmountable variable when studying a dynamic biofilm where cells exit the biofilm by various mechanisms (e.g., phase variation or fluid shear stress).

The reduced ability of Δ*chiA-1/A*-2 to increase in biomass on the chitin surface suggests that no other nutritional sources were present to sustain the growth and development of the *V. cholerae* biofilm. In our laminar flow system, the shift in chitin-specific growth after switching to non-nutritional media suggests that (i) any diffusion of nutrients from the chitin surface does not reach the glass in adequate amounts to sustain growth on the glass and (ii) any residual carbon [from initial $(GlcNAc)_2$ supplementation] or other contaminants during flow cell construction are also insufficient to sustain growth. The chemostat and laminar flow systems described here were successful in creating chitin-specific growth by cells that were previously exposed to $(GlcNAc)_2$, in a manner similar to that found in nature as cells migrate from various chitinous nutrient sources which they colonize or originate from.

The biphasic nature of N16961 biofilm development on artificial chitin resembled *V. cholerae* biofilm development on crab carapaces. Spatial differentiation took place within the initial monolayers as microcolonies developed while isolated cells remained present and evenly distributed. Microcolonies likely developed by clonal expansion of pioneering cells, but taxis to the surface by planktonic cells (randomly or by chemotactic means) may also have occurred. Real-time experiments and multi-colored labeling of

cells tracking the development of the initial monolayer could determine the origins of the biofilm communities.

One noteworthy feature of the biphasic monolayer is the pitting of microcolonies beneath the chitin surface under flow conditions. Pitting caused by cell clumps and microcolonies in the surface of artificial chitin may serve to maximize nutritional availability (by increasing exposure to the surface area) while protecting the colony from turbulent flow at the surface level. There is likely a limit to the height of microcolonies as they increase in density until complex structures are formed. Evidence of empty pits lined with cells as well as clumps of cells partially detached from the pits (observed at various timepoints in the chemostat experiments) indicate that cell-cell interactions confer stability to the microcolony and that the cell-cell interactions differ than the cell-surface interactions. It will be of great interest to compare attachment stability to artificial chitin with other chitinous surfaces of varied chemical compositions. Proteins, carbohydrates and other ligands may allow stronger cell-surface attachments as the substrate is destabilized by enzymatic degradation.

We have also demonstrated for the first time a non-ChiS mediated pathway for chitin utilization on artificial chitin in chemostatic flow conditions. Δ*chiS* biofilm development, albeit slower than wild-type, indicated that chitin sensing through a functional ChiS is not a requirement for chitin utilization; an alternate pathway of sensing and induction of chitin catabolic genes must exist for chitin utilization. The less robust biofilm of Δ*chiS* (relative to wild-type) lacked pitting colonies and displayed smooth colony morphology. The smoothness of these biofilms suggests that *vps* genes are not

induced without ChiS. Future expression analyses of Δ*chiS* biofilm will reveal the genes expressed in the non-ChiS dependent pathway.

In understanding *V. cholerae* biofilm development, it is important to consider the natural frameshift in the quorum sensing regulator, HapR, in N16961. This frameshift is thought to be an evolutionary adaptation to stressful environments as down-regulation of HapR leads to enhanced survivability, colonization, and thicker biofilms in the host (64). Induction of *hapR* occurs during quorum sensing when cell densities increase and make it favorable for cells to detach. Repression of HapR has been shown to induce expression of *vps* genes and is proposed to reduce cell exit from biofilms. N16961, then, may be more sensitive to environmental cues and may be more fit for environmental survival than strains with wild-type *hapR*. On the other hand, N16961 may be less responsive to high cell densities and produce less planktonic cells to exit the biofilm and relocate to a more favorable environment. Fitness studies using mutant N16961 carrying wild-type *hapR* may reveal the advantages and disadvantages of a less functional HapR.

Though complex and not well understood, rugosity is evidently regulated by environmental signals and is an important factor in chitin colonization. We observed smooth to rugose switching after the binding step (initial adhesion to the chitin), suggesting that incubation in the chemostats triggers switching to rugose. The switch to rugose has been shown to translate into increased VPS production and increased resistance to chlorine, osmotic and oxidative stress (36, 54). VPS synthesis may serve as nutrient storage for use during times of poor nutrient availability. The rugosity we observed within the biofilm-associated population in chemostats clearly shows that

rugosity persists during nutrient-rich conditions (indicated by thick biofilm). As mentioned previously, VPS production may also be a key factor in stabilizing cell-cell interactions and increase community survivability by conferring strength to biofilm-associated cells exposed to fluid shear stress in the chemostats. It is unknown whether the smooth and rugose cells are distributed evenly throughout the biofilm. The origin of smooth cells is also unknown; they may be derived from smooth cells (original inoculum) or from rugose cells that switched to back to smooth by phase variation.

Of course, our samples of planktonic cells do not reflect the true planktonic cell population as clumps of detached biofilm (caused by agitation of chemostats during sampling) could be present in unknown numbers. Instead, the planktonic cell counts offered a glimpse of the non-surface associated cell population during monolayer development and biofilm maturation. Future experiments should address the problem in quantifying planktonic cells in chemostats and account for clumps and individual cells that naturally detach in flow conditions by virtue of shearing stress and/or senescence within the biofilm. Methods should also be modified to capture the population of planktonic cells that exit the biofilm due to environmental and cell-cell signals.

Lastly, we demonstrated filamentous cell morphology during biofilm development on artificial chitin in laminar flow cells (Fig. 15). Differentiation of cell morphology may reflect an adaptive strategy and survival mechanism of N16961; filamentous cells remained attached to the chitin surface while the fully developed biofilm had sloughed away. The molecular and physiological events leading to filamentous cell differentiation are unknown. Possible reasons for differentiation into

filamentous cells include: (i) specialized function of filamentous cells in biofilm structure; (ii) nutritional limitations (e.g., amino acid deficiency) eliciting failure to septate; and (iii) cellular response to the surface or environment. The latter possibility relates to the observation of *E. coli* and *Salmonella typhimurium* differentiation into elongated nonspetate (filamentous) swarmer cells in response to various surface environments and nutritional conditions (25). Understanding this change in cell morphology will require the isolation of filamentous cells for further study. Nutritional experiments and expression analyses of filamentous isolates may give insight into the causes and mechanisms of morphological differentiation. Future studies using *gfp*-labeled cells should account for the unknown effects of *gfp* insertion on cell morphology and incorporate unlabeled strains as an experimental control.

Individual cells and communities must adapt to changes in temperature, salinity and chemical composition of their surroundings, in addition to competing intra- and interspecies symbionts within aquatic biofilms. In light of this, we must take into account phase variation in relation to environmental signals and community dynamics, which confer plasticity to biofilms and promote survival. Also, biofilm development may be regulated by signaling processes within communities to promote survival of individual members or communities as whole. Further investigation of the environmental signals, physiological processes, and regulatory mechanisms governing biofilm development will be essential to understanding *V. cholerae* survival in aquatic niches.

REFERENCES

1. **Ali, A., M. H. Rashid, and D. K. Karaolis.** 2002. High-frequency rugose exopolysaccharide production by Vibrio cholerae. Appl Environ Microbiol **68:**5773-8.

2. **Bassler, B. L., P. J. Gibbons, C. Yu, and S. Roseman.** 1991. Chitin utilization by marine bacteria. Chemotaxis to chitin oligosaccharides by Vibrio furnissii. J Biol Chem **266:**24268-75.

3. **Baty, A. M., 3rd, C. C. Eastburn, S. Techkarnjanaruk, A. E. Goodman, and G. G. Geesey.** 2000. Spatial and temporal variations in chitinolytic gene expression and bacterial biomass production during chitin degradation. Appl Environ Microbiol **66:**3574-85.

4. **Binsztein, N., M. C. Costagliola, M. Pichel, V. Jurquiza, F. C. Ramirez, R. Akselman, M. Vacchino, A. Huq, and R. Colwell.** 2004. Viable but nonculturable Vibrio cholerae O1 in the aquatic environment of Argentina. Appl Environ Microbiol **70:**7481-6.

5. **Blake, P. A., D. T. Allegra, J. D. Snyder, T. J. Barrett, L. McFarland, C. T. Caraway, J. C. Feeley, J. P. Craig, J. V. Lee, N. D. Puhr, and R. A. Feldman.** 1980. Cholera--a possible endemic focus in the United States. N Engl J Med **302:**305-9.

6. **Carman, K. R., and F. C. Dobbs.** 1997. Epibiotic microorganisms on copepods and other marine crustaceans. Microsc Res Tech **37:**116-35.

7. **Castro-Rosas, J., and E. F. Escartin.** 2002. Adhesion and colonization of Vibrio cholerae O1 on shrimp and crab carapaces. J Food Prot **65:**492-8.

8. **Chaiyanan, S., S. Chaiyanan, A. Huq, T. Maugel, and R. R. Colwell.** 2001. Viability of the nonculturable Vibrio cholerae O1 and O139. Syst Appl Microbiol **24:**331-41.

9. **Chakraborty, S., A. K. Mukhopadhyay, R. K. Bhadra, A. N. Ghosh, R. Mitra, T. Shimada, S. Yamasaki, S. M. Faruque, Y. Takeda, R. R. Colwell, and G. B. Nair.** 2000. Virulence genes in environmental strains of Vibrio cholerae. Appl Environ Microbiol **66:**4022-8.

10. **Chiavelli, D. A., J. W. Marsh, and R. K. Taylor.** 2001. The mannose-sensitive hemagglutinin of Vibrio cholerae promotes adherence to zooplankton. Appl Environ Microbiol **67:**3220-5.

11. **Colwell, R. R.** 1996. Global climate and infectious disease: the cholera paradigm. Science **274:**2025-31.

12. **Colwell, R. R.** 2000. Viable but nonculturable bacteria: a survival strategy. J Infect Chemother **6:**121-5.

13. **Colwell, R. R. (ed.).** 1984. Vibrios in the Environment. John Wiley & Sons Inc.

14. **Compere, P., M. F. Jaspar-Versali, and G. Goffinet.** 2002. Glycoproteins from the cuticle of the Atlantic shore crab Carcinus maenas: I. Electrophoresis and Western-blot analysis by use of lectins. Biol Bull **202:**61-73.

15. **Cook, D. W., and S. R. Lofton.** 1973. Chitinoclastic bacteria associated with shell disease in Penaeus shrimp and the blue crab (Callinectes sapidus). J Wildl Dis **9:**154-9.

16. **Dang, H., and C. R. Lovell.** 2000. Bacterial primary colonization and early succession on surfaces in marine waters as determined by amplified rRNA gene restriction analysis and sequence analysis of 16S rRNA genes. Appl Environ Microbiol **66:**467-75.

17. **Davey, M. E., and A. O'Toole G.** 2000. Microbial biofilms: from ecology to molecular genetics. Microbiol Mol Biol Rev **64:**847-67.

18. **Faruque, S. M., G. B. Nair, and J. J. Mekalanos.** 2004. Genetics of stress adaptation and virulence in toxigenic Vibrio cholerae. DNA Cell Biol **23:**723-41.

19. **Finelli, L., D. Swerdlow, K. Mertz, H. Ragazzoni, and K. Spitalny.** 1992. Outbreak of cholera associated with crab brought from an area with epidemic disease. J Infect Dis **166:**1433-5.

20. **Gabreiel Bitton, K. C. M.** 1980. Adsorption of Microorganisms to Surfaces. Wiley, New York.

21. **Garay, E., A. Arnau, and C. Amaro.** 1985. Incidence of Vibrio cholerae and related vibrios in a coastal lagoon and seawater influenced by lake discharges along an annual cycle. Appl Environ Microbiol **50:**426-30.

22. **Geesey, G. G.** 2001. Bacterial behavior at surfaces. Curr Opin Microbiol **4:**296-300.

23. **Guthmann, J. P.** 1995. Epidemic cholera in Latin America: spread and routes of transmission. J Trop Med Hyg **98:**419-27.

24. **Hammer, B. K., and B. L. Bassler.** 2003. Quorum sensing controls biofilm formation in Vibrio cholerae. Mol Microbiol **50:**101-4.

25. **Harshey, R. M., and T. Matsuyama.** 1994. Dimorphic transition in Escherichia coli and Salmonella typhimurium: surface-induced differentiation into hyperflagellate swarmer cells. Proc Natl Acad Sci U S A **91:**8631-5.

26. **Heidelberg, J. F., K. B. Heidelberg, and R. R. Colwell.** 2002. Bacteria of the gamma-subclass Proteobacteria associated with zooplankton in Chesapeake Bay. Appl Environ Microbiol **68:**5498-507.

27. **Huq, A., S. A. Huq, D. J. Grimes, M. O'Brien, K. H. Chu, J. M. Capuzzo, and R. R. Colwell.** 1986. Colonization of the gut of the blue crab (Callinectes sapidus) by Vibrio cholerae. Appl Environ Microbiol **52:**586-8.

28. **Huq, A., E. B. Small, P. A. West, M. I. Huq, R. Rahman, and R. R. Colwell.** 1983. Ecological relationships between Vibrio cholerae and planktonic crustacean copepods. Appl Environ Microbiol **45:**275-83.

29. **Karaolis, D. K., R. Lan, and P. R. Reeves.** 1995. The sixth and seventh cholera pandemics are due to independent clones separately derived from environmental, nontoxigenic, non-O1 Vibrio cholerae. J Bacteriol **177:**3191-8.

30. **Keyhani, N. O., and S. Roseman.** 1999. Physiological aspects of chitin catabolism in marine bacteria. Biochim Biophys Acta **1473:**108-22.

31. **Kumari, S. S., J. H. Willis, and D. M. Skinner.** 1995. Proteins of crustacean exoskeleton: IV. Partial amino acid sequences of exoskeletal proteins from the Bermuda land crab, Gecarcinus lateralis, and comparisons to certain insect proteins. J Exp Zool **273:**389-400.

32. **Li, X., and S. Roseman.** 2004. The chitinolytic cascade in Vibrios is regulated by chitin oligosaccharides and a two-component chitin catabolic sensor/kinase. Proc Natl Acad Sci U S A **101:**627-31.

33. **Lipp, E. K., A. Huq, and R. R. Colwell.** 2002. Effects of global climate on infectious disease: the cholera model. Clin Microbiol Rev **15:**757-70.

34. **Meibom, K. L., X. B. Li, A. T. Nielsen, C. Y. Wu, S. Roseman, and G. K. Schoolnik.** 2004. The Vibrio cholerae chitin utilization program. Proc Natl Acad Sci U S A **101:**2524-9.

35. **Miller, M. B., K. Skorupski, D. H. Lenz, R. K. Taylor, and B. L. Bassler.** 2002. Parallel quorum sensing systems converge to regulate virulence in Vibrio cholerae. Cell **110:**303-14.

36. **Morris, J. G., Jr., M. B. Sztein, E. W. Rice, J. P. Nataro, G. A. Losonsky, P. Panigrahi, C. O. Tacket, and J. A. Johnson.** 1996. Vibrio cholerae O1 can assume a chlorine-resistant rugose survival form that is virulent for humans. J Infect Dis **174:**1364-8.

37. **Nalin, D. R., V. Daya, A. Reid, M. M. Levine, and L. Cisneros.** 1979. Adsorption and growth of Vibrio cholerae on chitin. Infect Immun **25:**768-70.

38. **O'Brien, J., S. S. Kumari., and D. M. Skinner.** 1991. Proteins of crustacean exoskeletons: I. Similarities and differences among proteins of the four exoskeletal layers of four Brachyurans. Biol Bull **181:**427-441.

39. **Otto, K., and T. J. Silhavy.** 2002. Surface sensing and adhesion of Escherichia coli controlled by the Cpx-signaling pathway. Proc Natl Acad Sci U S A **99:**2287-92.

40. **Ramamurthy, T., S. Yamasaki, Y. Takeda, and G. B. Nair.** 2003. Vibrio cholerae O139 Bengal: odyssey of a fortuitous variant. Microbes Infect **5:**329-44.

41. **Reguera, G., and R. Kolter.** 2005. Virulence and the environment: a novel role for Vibrio cholerae toxin-coregulated pili in biofilm formation on chitin. J Bacteriol **187:**3551-5.

42. **Reisner, A., J. A. Haagensen, M. A. Schembri, E. L. Zechner, and S. Molin.** 2003. Development and maturation of Escherichia coli K-12 biofilms. Mol Microbiol **48:**933-46.

43. **Riemann, L., and F. Azam.** 2002. Widespread N-acetyl-D-glucosamine uptake among pelagic marine bacteria and its ecological implications. Appl Environ Microbiol **68:**5554-62.

44. **Sack, D. A., R. B. Sack, G. B. Nair, and A. K. Siddique.** 2004. Cholera. Lancet **363:**223-33.

45. **Singh, D. V., M. H. Matte, G. R. Matte, S. Jiang, F. Sabeena, B. N. Shukla, S. C. Sanyal, A. Huq, and R. R. Colwell.** 2001. Molecular analysis of Vibrio cholerae O1, O139, non-O1, and non-O139 strains: clonal relationships between clinical and environmental isolates. Appl Environ Microbiol **67:**910-21.

46. **Stanley, N. R., and B. A. Lazazzera.** 2004. Environmental signals and regulatory pathways that influence biofilm formation. Mol Microbiol **52:**917-24.

47. **Suginta, W., P. A. Robertson, B. Austin, S. C. Fry, and L. A. Fothergill-Gilmore.** 2000. Chitinases from Vibrio: activity screening and purification of chiA from Vibrio carchariae. J Appl Microbiol **89:**76-84.

48. **Tamplin, M. L., A. L. Gauzens, A. Huq, D. A. Sack, and R. R. Colwell.** 1990. Attachment of Vibrio cholerae serogroup O1 to zooplankton and phytoplankton of Bangladesh waters. Appl Environ Microbiol **56:**1977-80.

49. **Tarsi, R., and C. Pruzzo.** 1999. Role of surface proteins in Vibrio cholerae attachment to chitin. Appl Environ Microbiol **65:**1348-51.

50. **Taylor, R. K.** 1991. Bacterial adhesion to mucosal surfaces. J Chemother **3 Suppl 1:**190-5.

51. **Taylor, R. K., V. L. Miller, D. B. Furlong, and J. J. Mekalanos.** 1987. Use of phoA gene fusions to identify a pilus colonization factor coordinately regulated with cholera toxin. Proc Natl Acad Sci U S A **84:**2833-7.

52. **Thompson, F. L., T. Iida, and J. Swings.** 2004. Biodiversity of vibrios. Microbiol Mol Biol Rev **68:**403-31, table of contents.

53. **Vogan, C. L., C. Costa-Ramos, and A. F. Rowley.** 2002. Shell disease syndrome in the edible crab, Cancer pagurus--isolation, characterization and pathogenicity of chitinolytic bacteria. Microbiology **148:**743-54.

54. **Wai, S. N., Y. Mizunoe, A. Takade, S. I. Kawabata, and S. I. Yoshida.** 1998. Vibrio cholerae O1 strain TSI-4 produces the exopolysaccharide materials that determine colony morphology, stress resistance, and biofilm formation. Appl Environ Microbiol **64:**3648-55.

55. **Wai, S. N., Y. Mizunoe, and S. Yoshida.** 1999. How Vibrio cholerae survive during starvation. FEMS Microbiol Lett **180:**123-31.

56. **Waldor, M. K., and J. J. Mekalanos.** 1996. Lysogenic conversion by a filamentous phage encoding cholera toxin. Science **272:**1910-4.

57. **Watnick, P. I., K. J. Fullner, and R. Kolter.** 1999. A role for the mannose-sensitive hemagglutinin in biofilm formation by Vibrio cholerae El Tor. J Bacteriol **181:**3606-9.

58. **Watnick, P. I., and R. Kolter.** 1999. Steps in the development of a Vibrio cholerae El Tor biofilm. Mol Microbiol **34:**586-95.

59. **WHO.** 2003. Cholera, 2002. Weekly Epidemiological Record **78:**269-276.

60. **Williams, V., and M. Fletcher.** 1996. Pseudomonas fluorescens adhesion and transport through porous media are affected by lipopolysaccharide composition. Appl Environ Microbiol **62:**100-4.

61. **Yildiz, F. H., N. A. Dolganov, and G. K. Schoolnik.** 2001. VpsR, a Member of the Response Regulators of the Two-Component Regulatory Systems, Is Required for Expression of vps Biosynthesis Genes and EPS(ETr)-Associated Phenotypes in Vibrio cholerae O1 El Tor. J Bacteriol **183:**1716-26.

62. **Yildiz, F. H., and G. K. Schoolnik.** 1999. Vibrio cholerae O1 El Tor: identification of a gene cluster required for the rugose colony type, exopolysaccharide production, chlorine resistance, and biofilm formation. Proc Natl Acad Sci U S A **96:**4028-33.

63. **Yu, C., A. M. Lee, B. L. Bassler, and S. Roseman.** 1991. Chitin utilization by marine bacteria. A physiological function for bacterial adhesion to immobilized carbohydrates. J Biol Chem **266:**24260-7.

64. **Zhu, J., M. B. Miller, R. E. Vance, M. Dziejman, B. L. Bassler, and J. J. Mekalanos.** 2002. Quorum-sensing regulators control virulence gene expression in Vibrio cholerae. Proc Natl Acad Sci U S A **99:**3129-34.

Table 1. Bacterial strains and plasmids used in this study

Strain or plasmid	Characteristics[a]	Source or reference
Strains		
Vibrio cholerae		
N16961[b]	O1 El Tor, Sm^r	Laboratory strain
N16961Δ*pilA*	N196961 ΔVC2423	(34)
N16961Δ*msha*	N196961 ΔVC0409	(34)
N16961Δ*flaA*	N196961 ΔVC2188	Laboratory strain
N16961Δ*chiA-1A-2*[b]	N16961 ΔVC1952 ΔVCA0027	(34)
VCXB21[b]	N16961 ΔscrA ΔlacZ, Kan^r	(32)
VCXB21Δ*chiS*[b]	N16961 ΔscrA ΔlacZ, ΔVC0622, Kan^r	(32)
Escherichia coli		
S17-1	Donor strain carrying pGP704-Tn7	Laboratory strain
SM10	Helper strain carrying pUX-BF13	Laboratory strain
Plasmids		
pGP704-Tn7	Suicide vector (Tn7-GFP construct), Amp^r	Laboratory strain
pUX-BF13	Helper plasmid	Laboratory strain

[a] Sm^r, streptomycin resistance; Kan^r, kanamycin resistance; Amp^r, ampicillin resistance.

[b] recipient strains for chromosomal insertion of *gfp*.

Figure 1. Diagram of a chemostatic flow system. Chemostat is shown with slide and chitin mounts (green). Arrows indicate direction of media, air, and effluent flow. Air exits at the bottom of the chemostat behind slide and chitin mounts.

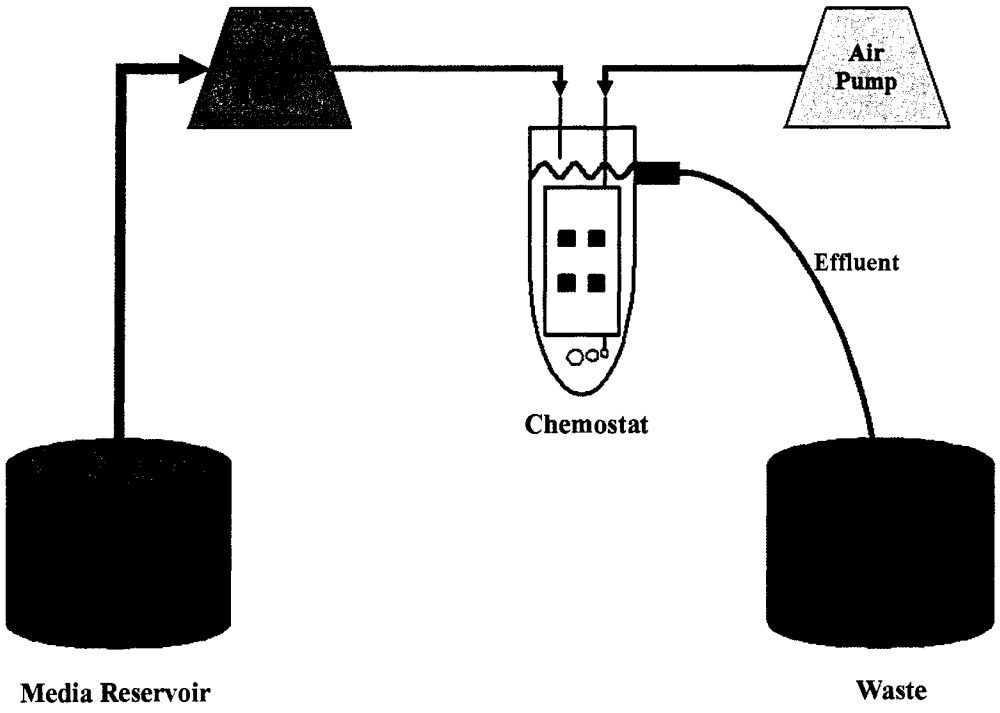

Figure 2. Diagram of a laminar flow cell. Sagittal section of a flow cell is shown with constitutive parts (A) and direction of media flow (B). Parts are labeled as follows: 1 = glass coverslip, 2 = chamber, 3 = artificial chitin, 4 = adhesive, 5 = coupon.

A)

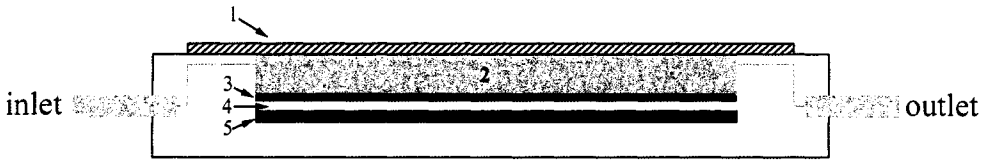

B)

Figure 3. Surface architecture of crab carapace. Scanning electron micrographs of topside (A) and underside (B) are shown. Scanning parameters, magnification, and scale bar are shown on the bottom of each micrograph. Surface features are labeled in red as follows: 1 = intact area, 2 = damaged area, 3 = shallow pit, 4 = crevice.

A. Topside

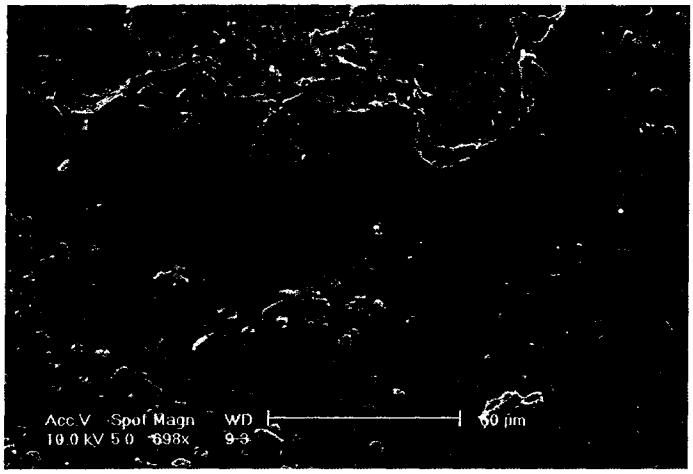

B. Underside

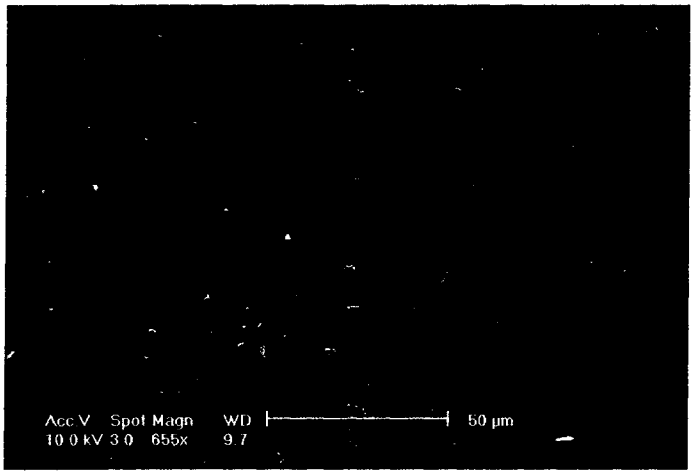

Figure 4, Plate 1. Timecourse of biofilm development on topside of crab carapace by N16961, Δ*pilA* and Δ*mshA*. Representative scanning electron micrographs of biofilm at 24-hour intervals from triplicate assays are shown. Scanning parameters, magnification, and scale bar are shown on the bottom of each micrograph.

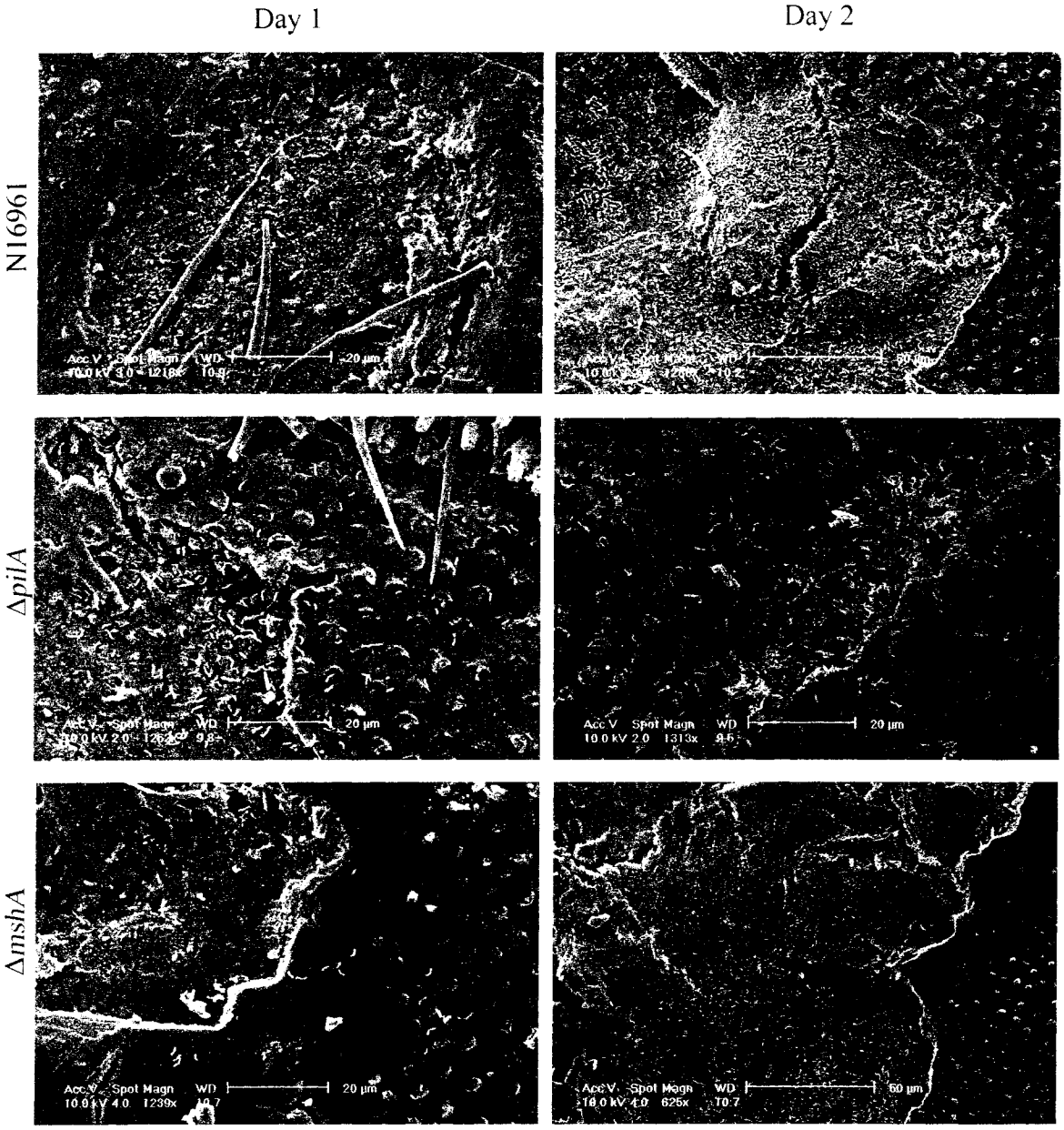

Figure 4, Plate 2.

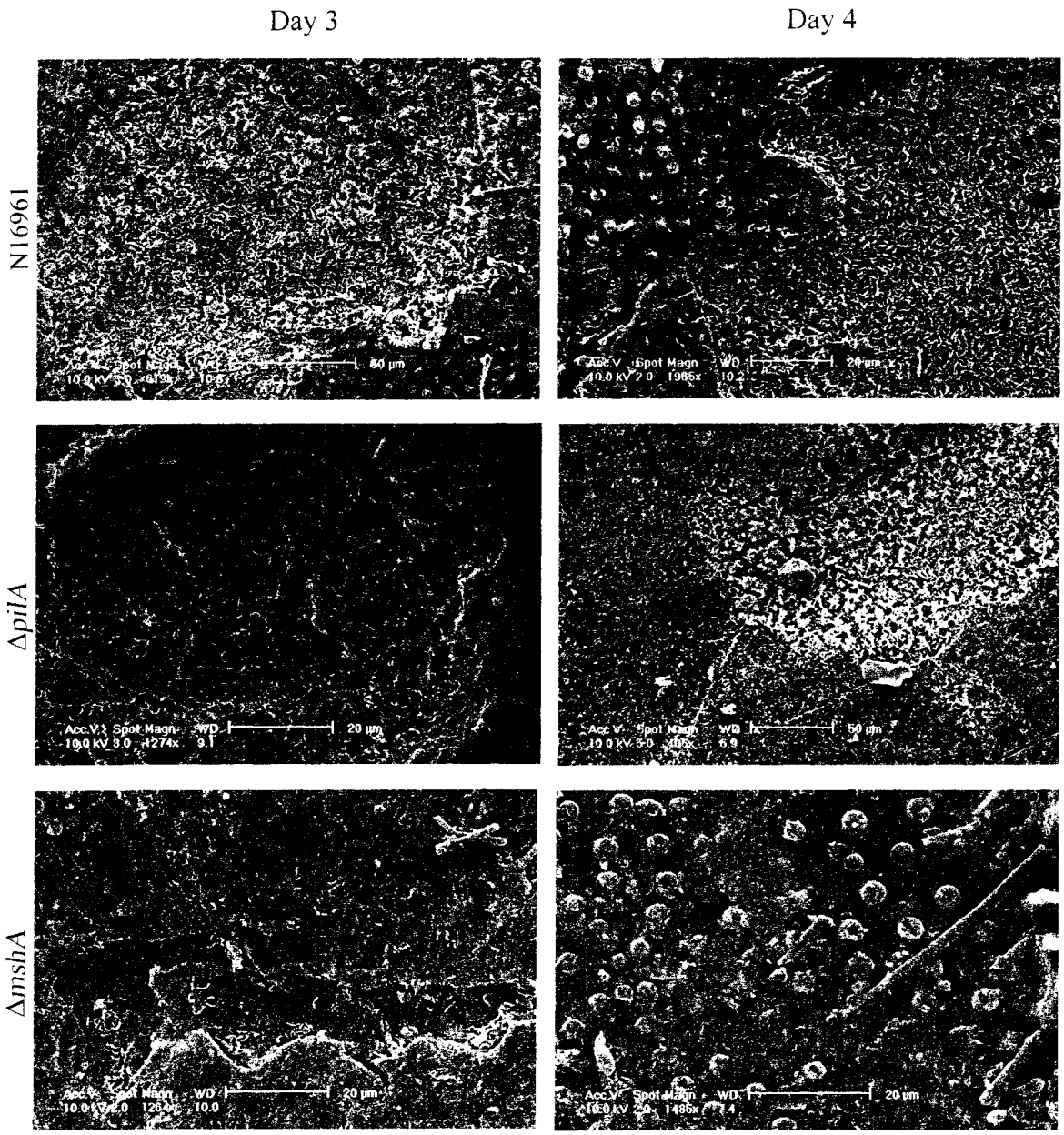

Figure 5, Plate 1. Timecourse of biofilm development on underside of crab carapace by N16961, Δ*pilA* and Δ*mshA*. Representative scanning electron micrographs of day 1, 2, 3, and 4 timepoints are shown. Scanning parameters, magnification, and scale bar are shown on the bottom of each micrograph.

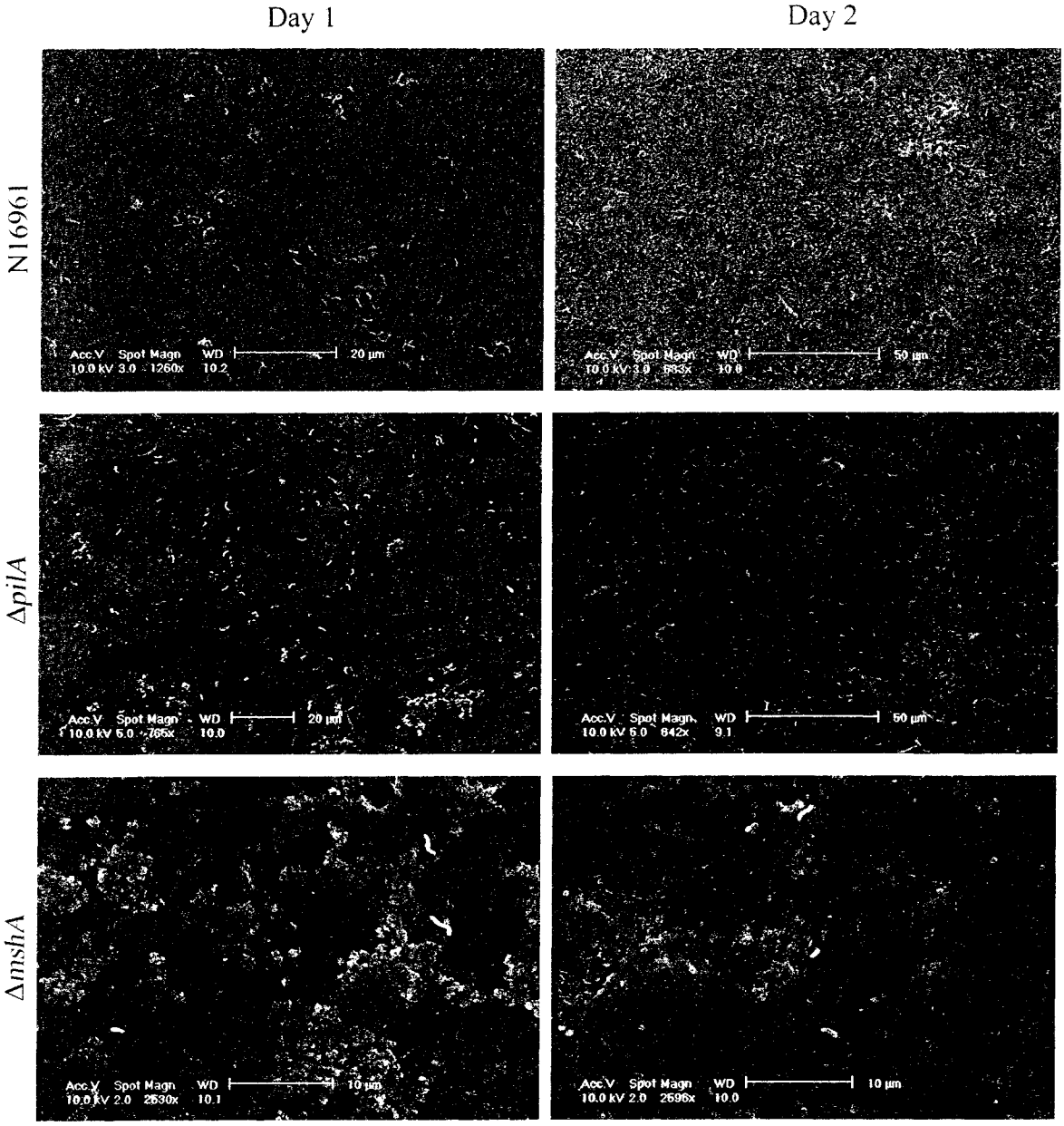

Figure 5, Plate 2.

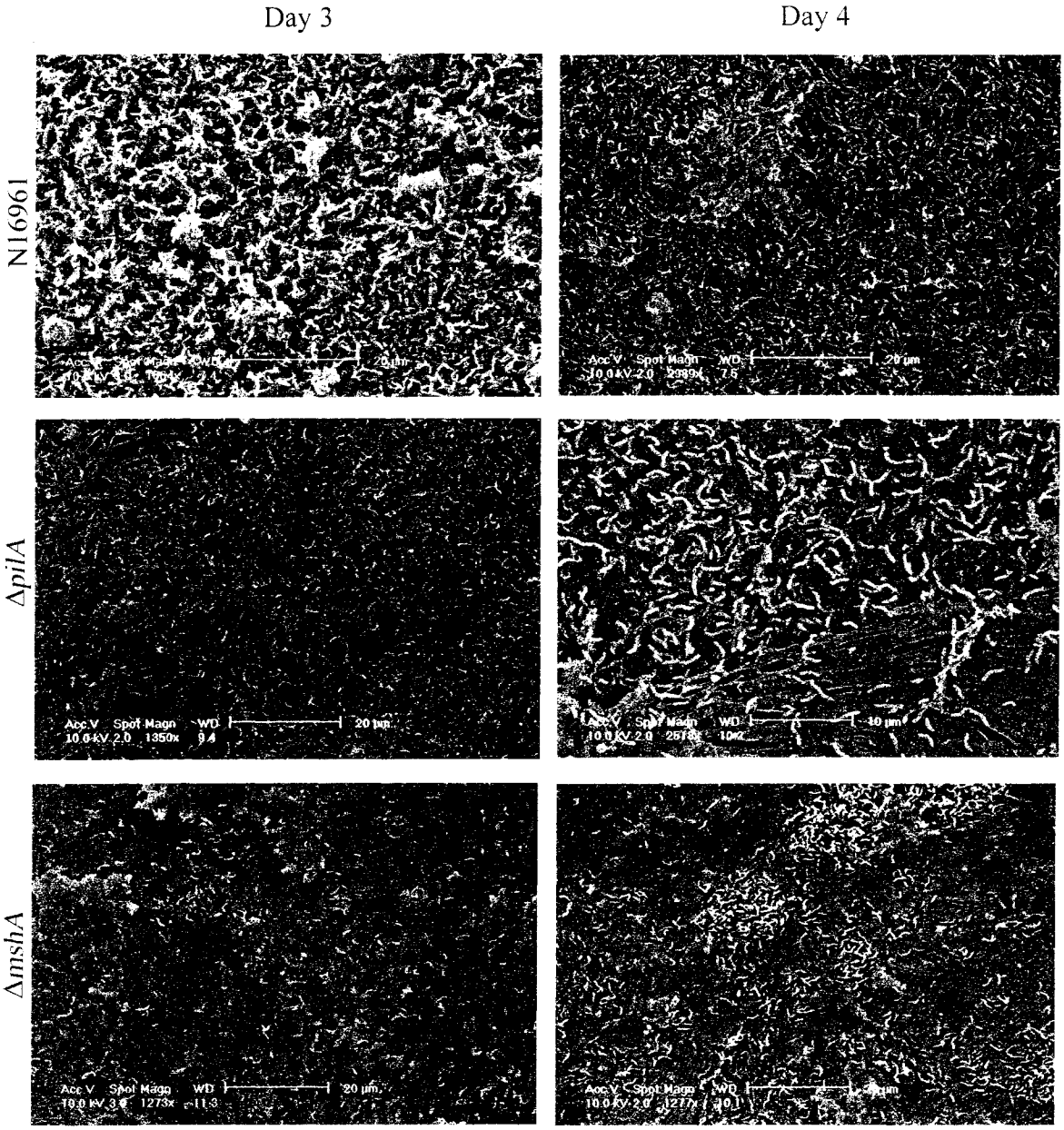

Figure 6. Timecourse of biofilm development on topside of crab carapace by N16961 and Δ*flaA*. Representative scanning electron micrographs of day 1, 2, and 3 timepoints are shown. Scanning parameters, magnification, and scale bar are shown on the bottom of each micrograph.

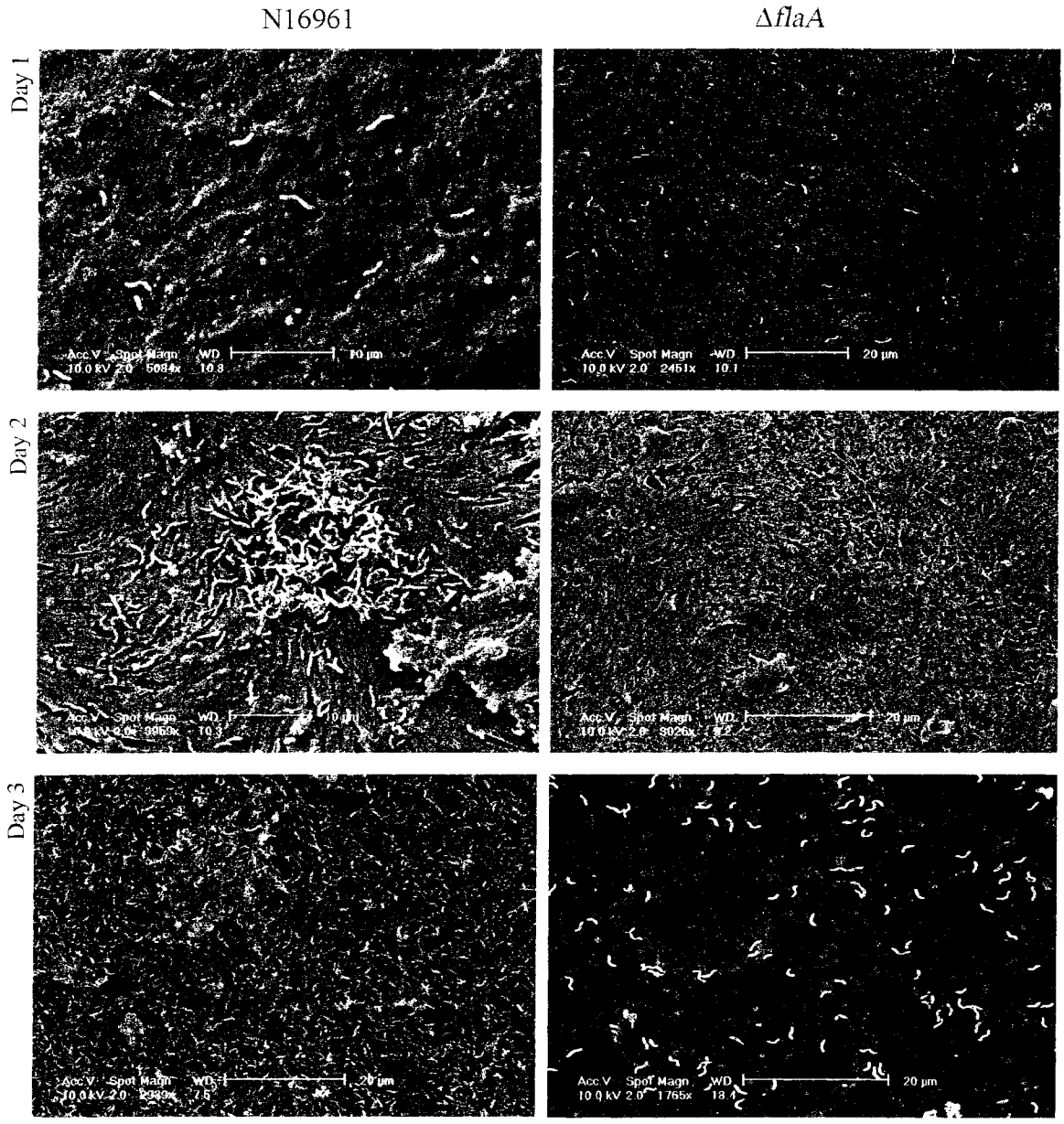

Figure 7, Plate 1. Colonization of crab carapace underside. Crab shells inoculated with N16961, Δ*pilA* , and Δ*mshA* were sampled after 48 hours incubation. Random areas were sampled by SEM at 2000× magniifcation. Percentages were based on the number of micrographs displaying monolayer containing ≥ 200 isolated cells (A) and number of micrographs with ≥ 1 micocolony (≥ 15 cells) present (B).

A)

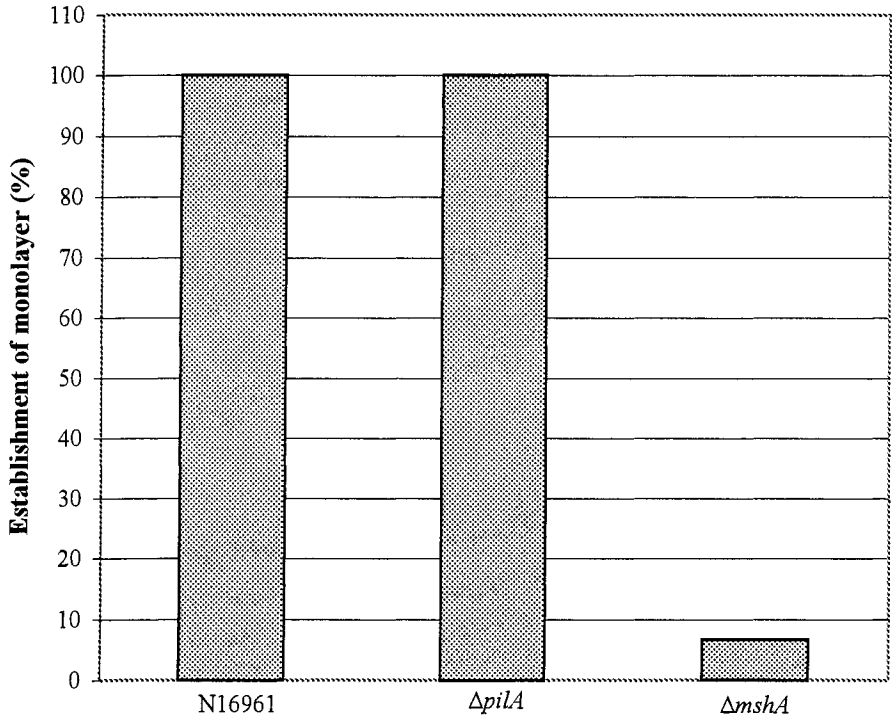

Figure 7, Plate 2.

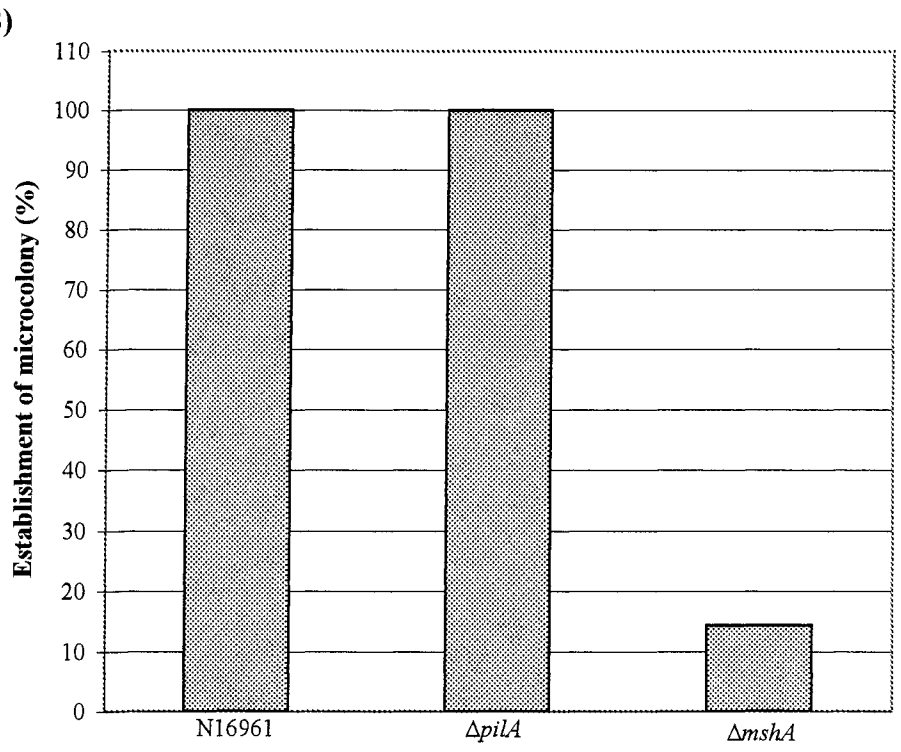

Figure 8, Plate 1. Timecourse of N16961 biofilm development on artificial chitin under chemostatic flow conditions. CSLM projections display *gfp*-labeled cells (green) on the chitin substratum (red) in *x*-*y* and selected *x*-*z* (top), *y*-*z* (right) saggital sections. Bar = 30 μm.

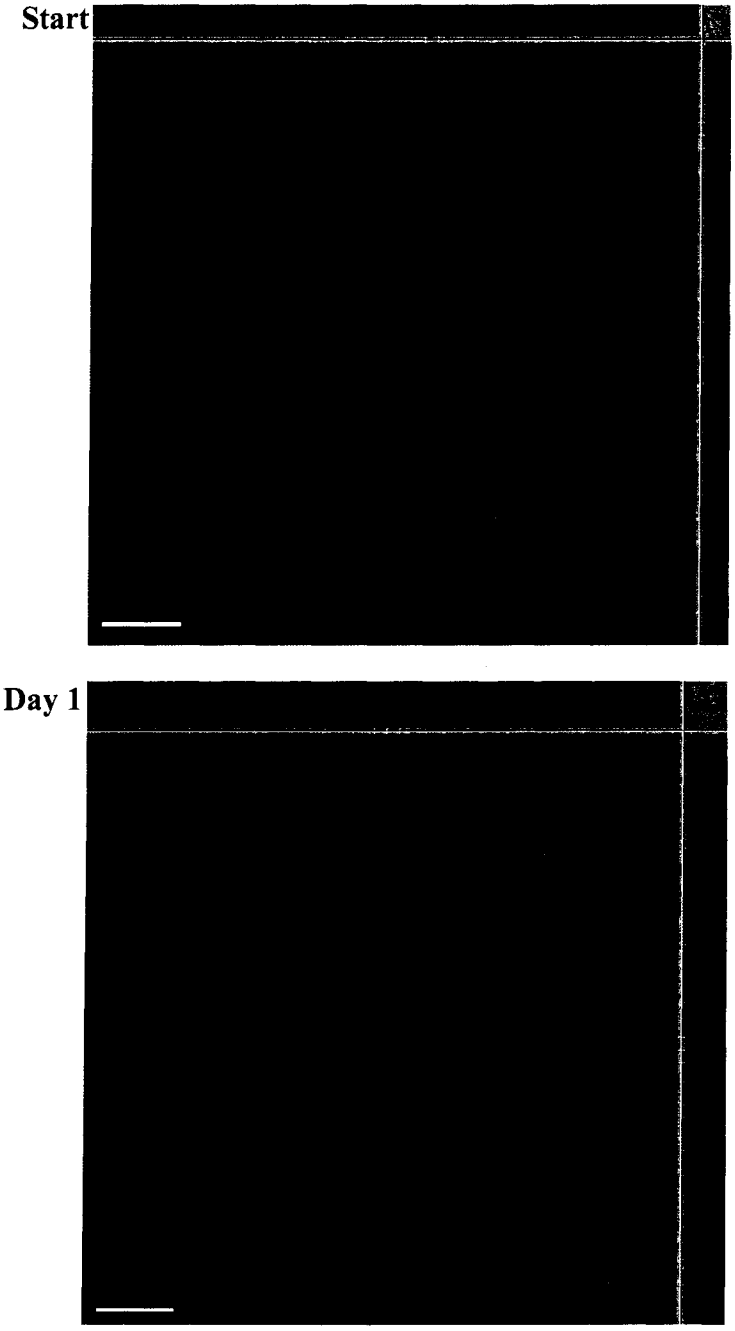

Figure 8, Plate 2.

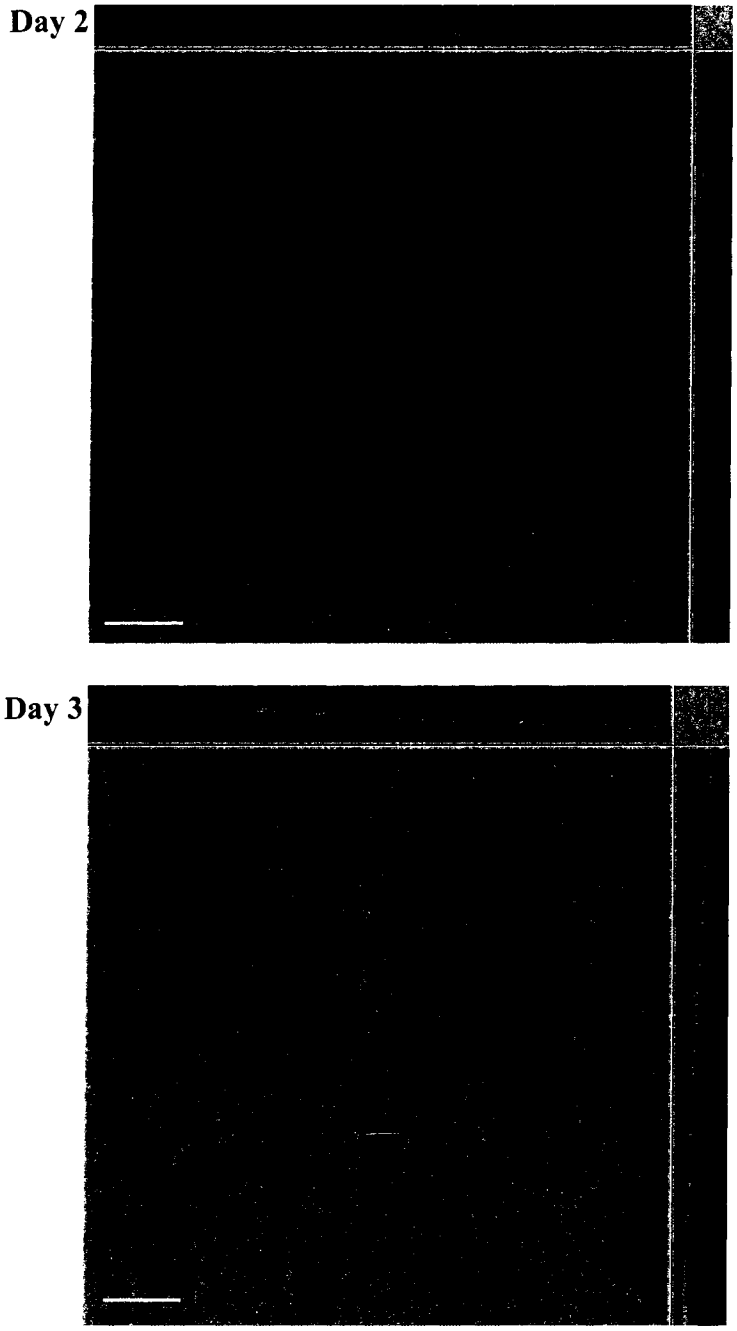

Figure 8, Plate 3.

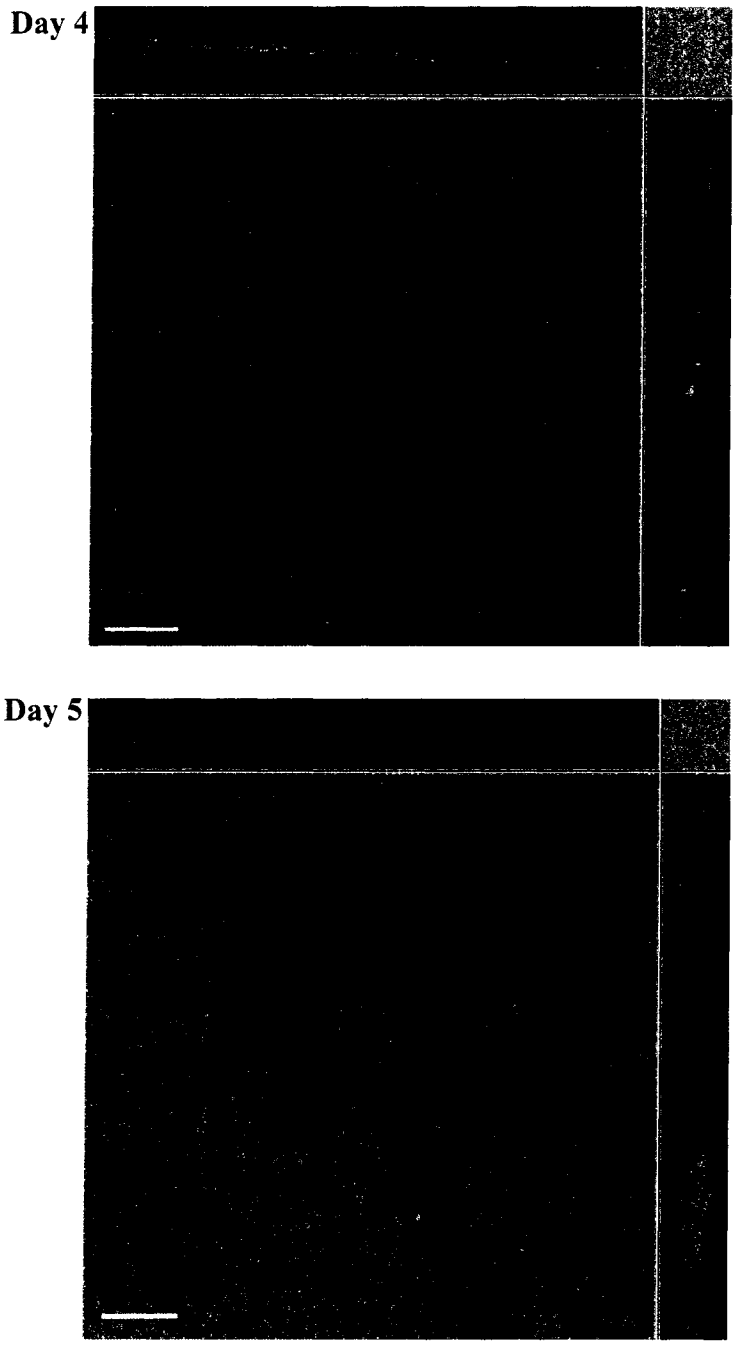

Figure 9, Plate 1. Timecourse of VCXB21 and Δ*chiS* biofilm development on artificial chitin under chemostatic flow conditions. CSLM projections display *gfp*-labeled cells (green) on chitin substratum (red) and glass (red) in *x*-*y* and selected *x*-*z* (top), *y*-*z* (right) saggital sections. Bar = 30 μm.

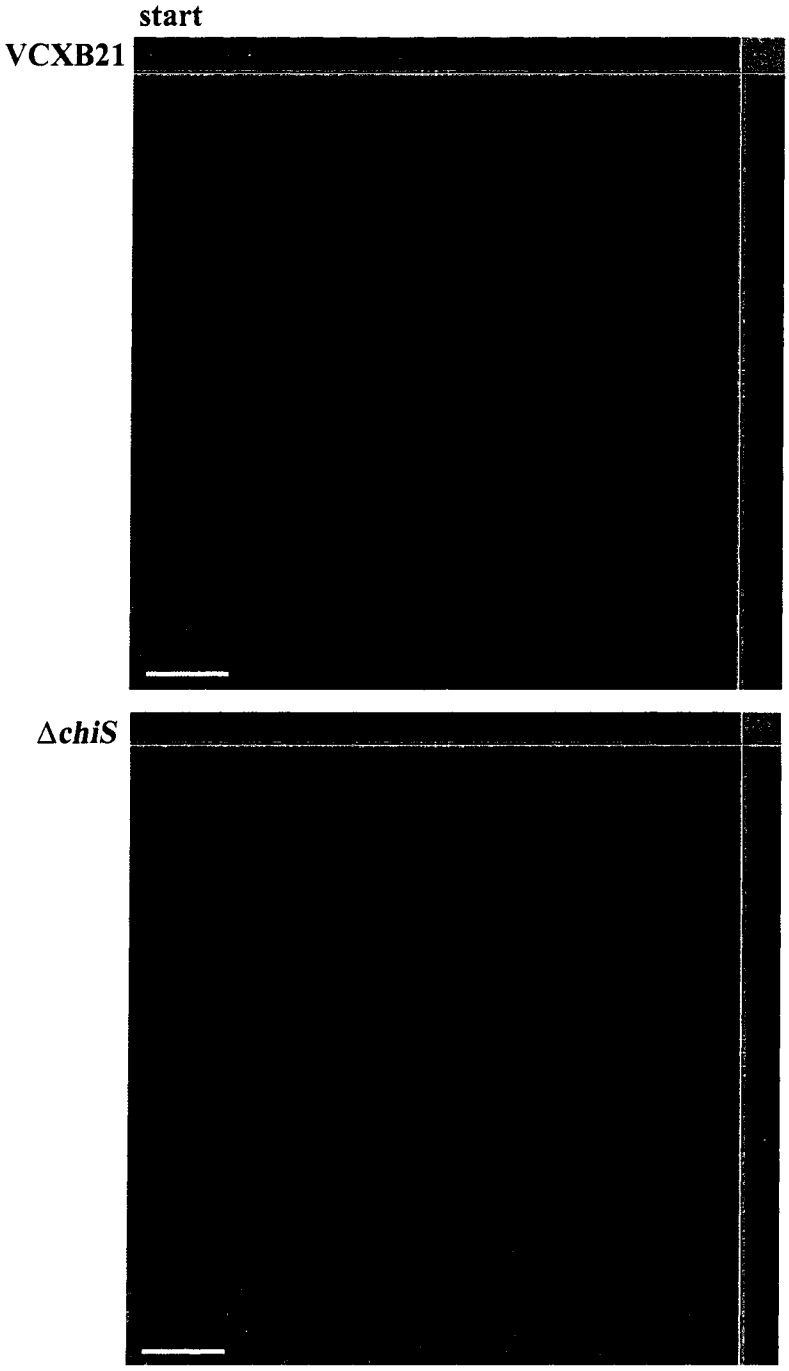

Figure 9, Plate 2.

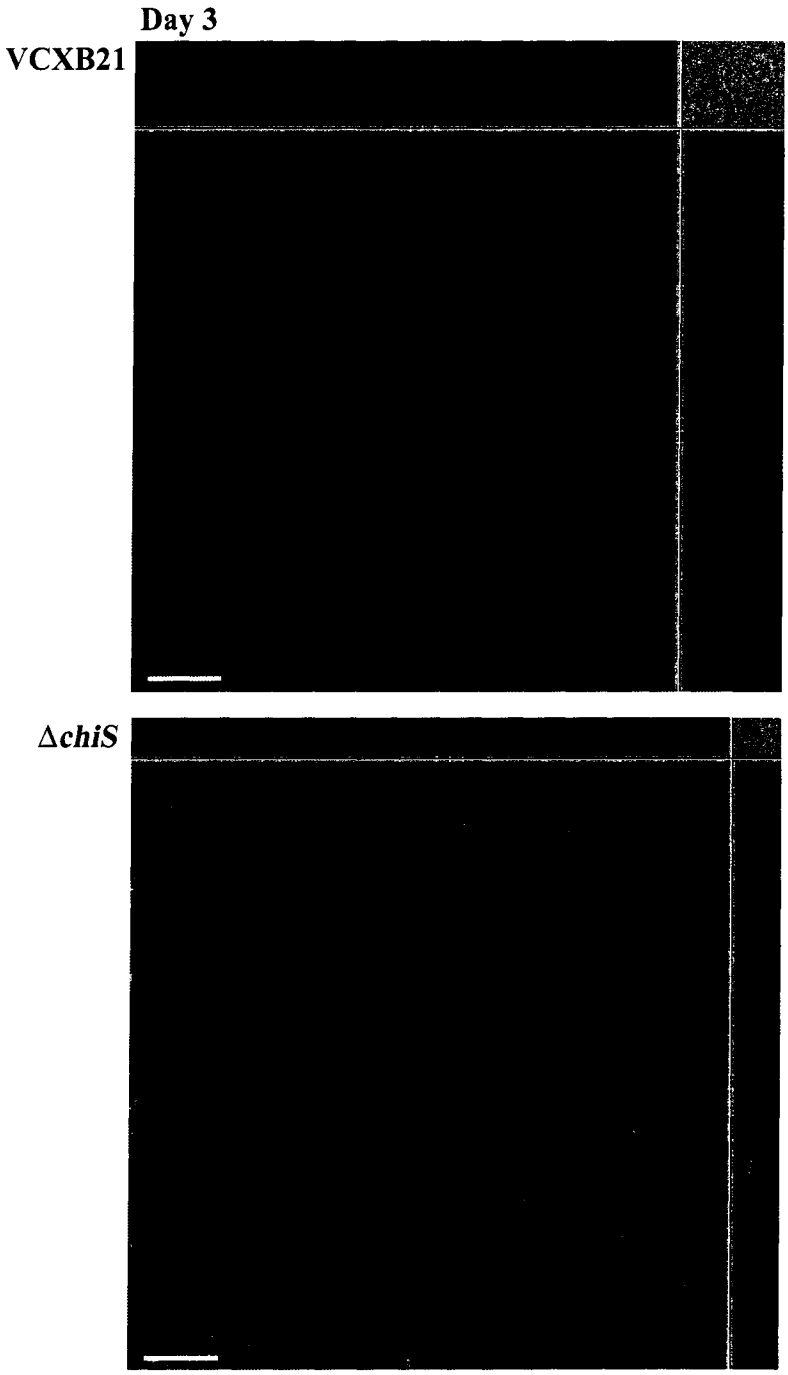

Figure 9, Plate 3.

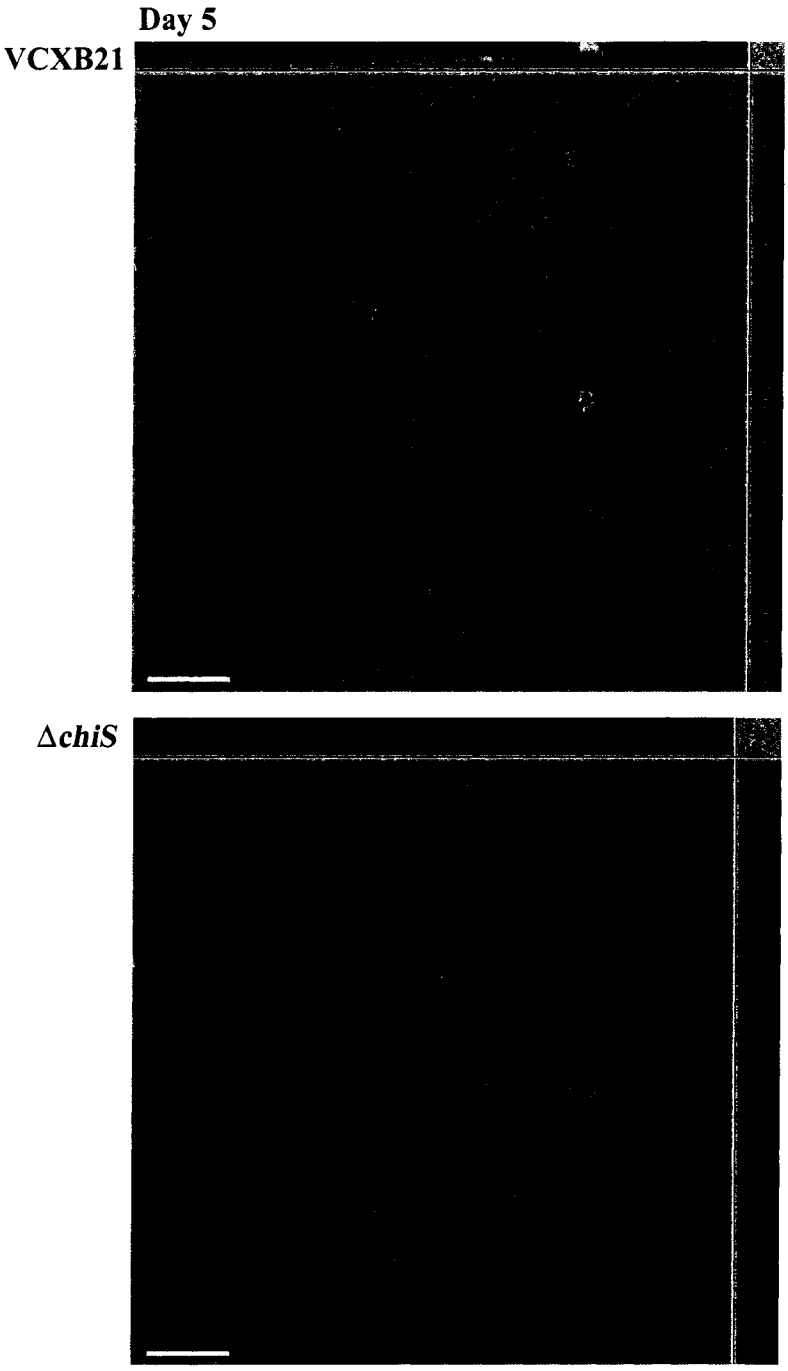

Figure 10, Plate 1. Chitin clearing by biofilm-accosiated cells from chemostats. N16961, Δ*chiA-1A-2*, VCXB21, and Δ*chiS* were harvested from chemostats and incubated on M9-chitin agar plates for 7 days. Representative plates are shown for each strain.

N16961

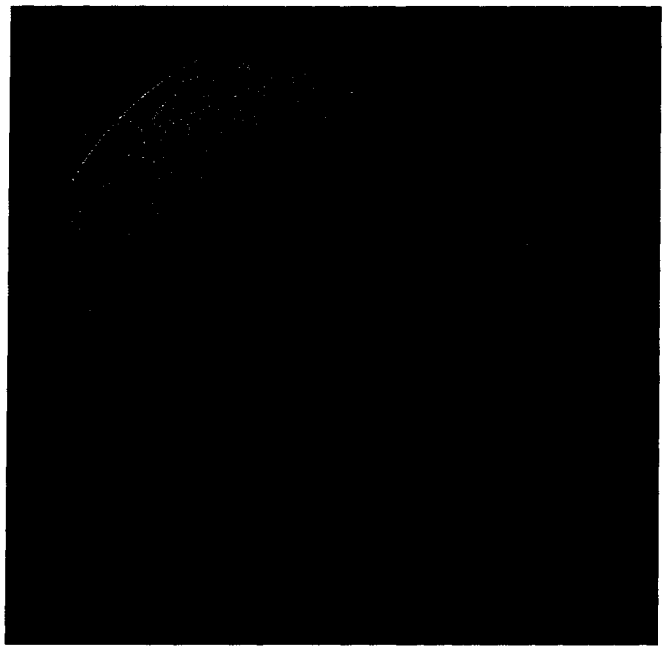

Δ*chiA-1A-2*

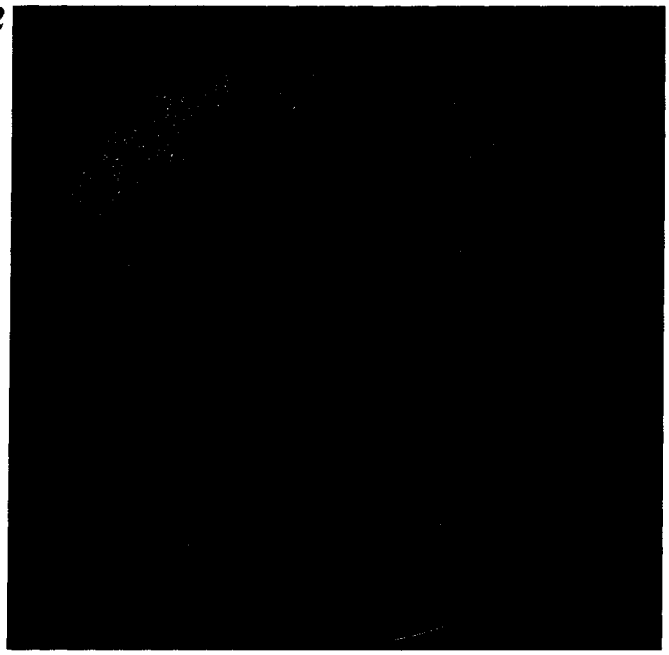

Figure 10, Plate 2.

VCXB21

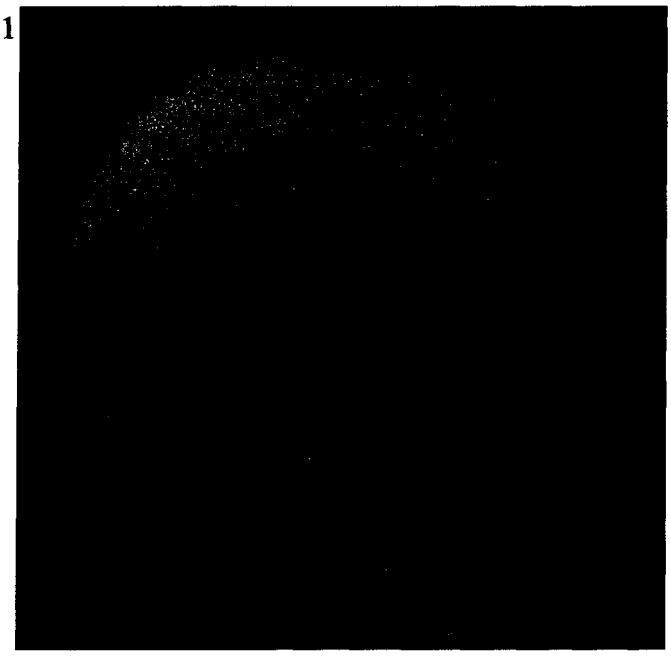

Δ*chiS*

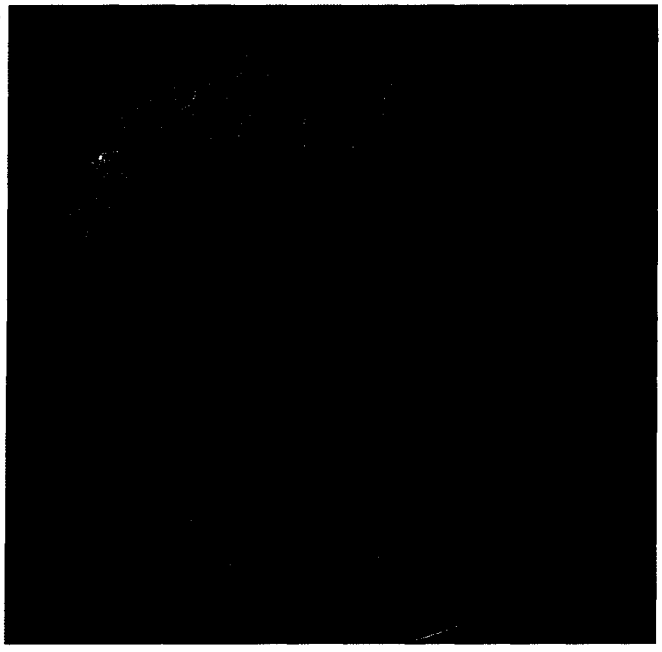

Figure 11. Rugosity during during N16961, Δ*chiA-1A-2*, VCXB21, and Δ*chiS* biofilm devlopment in chemostats. Percentages of rugose CFU of planktonic cells after 3 days (A) and biofilm-associated cells after 5 days (B) of incubation.

A) Planktonic cells

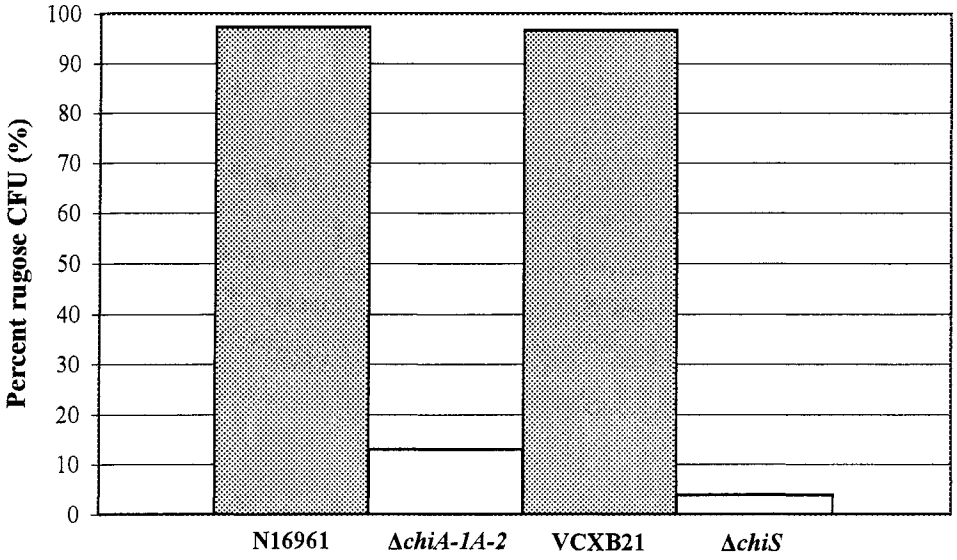

B) Biofilm-associated cells

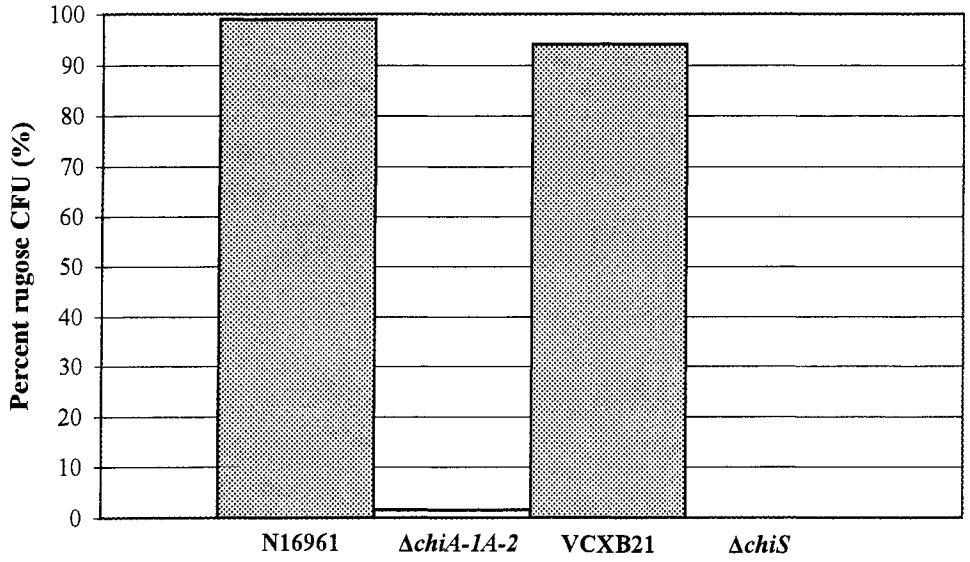

Figure 12. Comparison of chitin clearing by stock strains and experimental isolates. The following are shown after 5 days of incubation on M9-chitin agar: N16961 (stock), VCXB21 (stock), Δ*chiS* (stock), and experimental isolates (1-6) of Δ*chiS*.

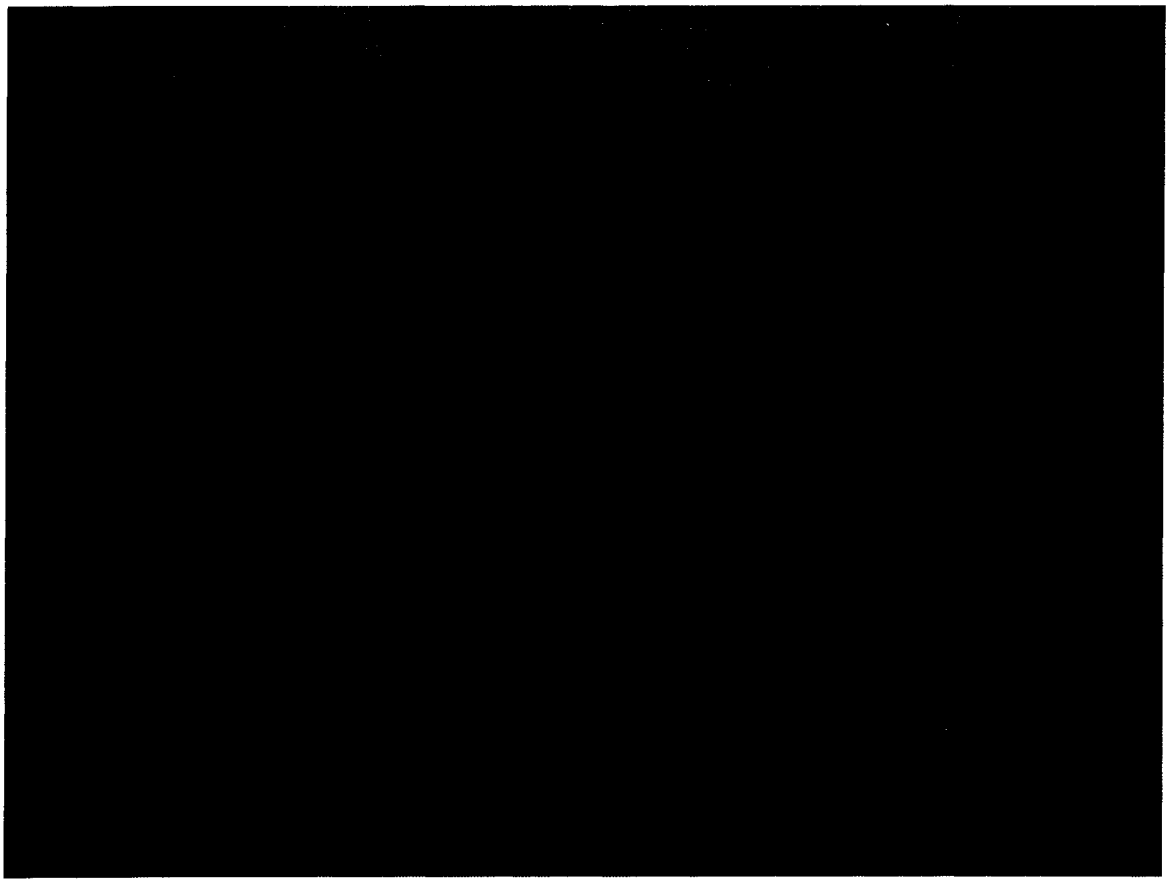

Figure 13, Plate 1. Effects of $(GlcNAc)_2$ on N16961 biofilm development on artificial chitin under chemostatic flow conditions. CSLM projections display *gfp*-labeled cells (green) on the chitin substratum (red) in *x-y* and selected *x-z* (top), *y-z* (right) saggital sections. Chemostats were given SDASW supplemented with 0.001% $(GlcNAc)_2$ for 12 hours (A), 24 hours (B), or SDASW alone (C). Bar = 30 μm.

Day 1

A)

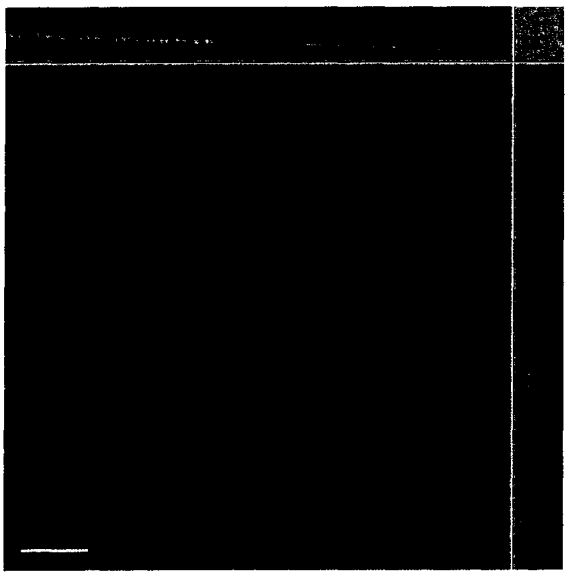

B)

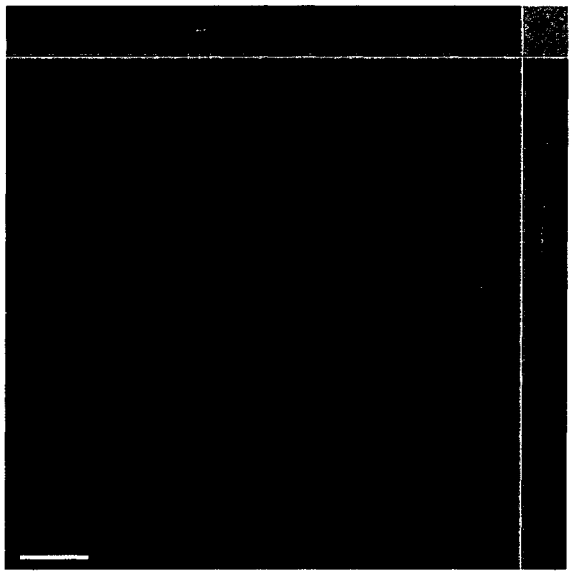

C)

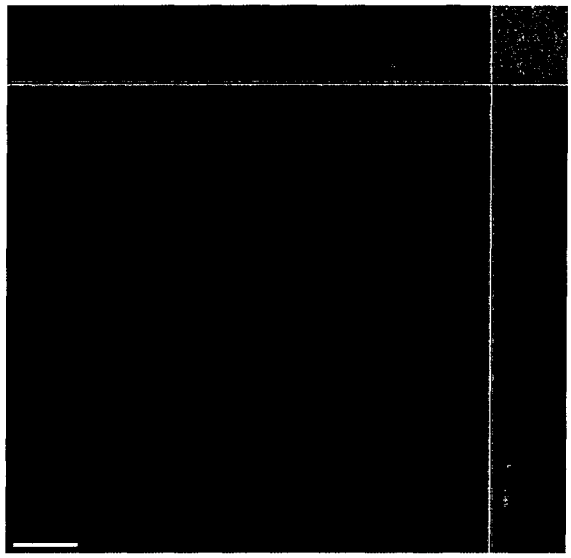

Figure 13, Plate 2.

Day 2

A)

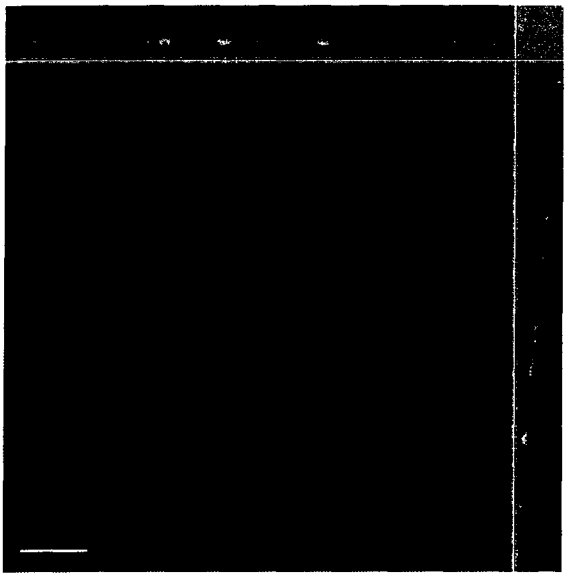

B)

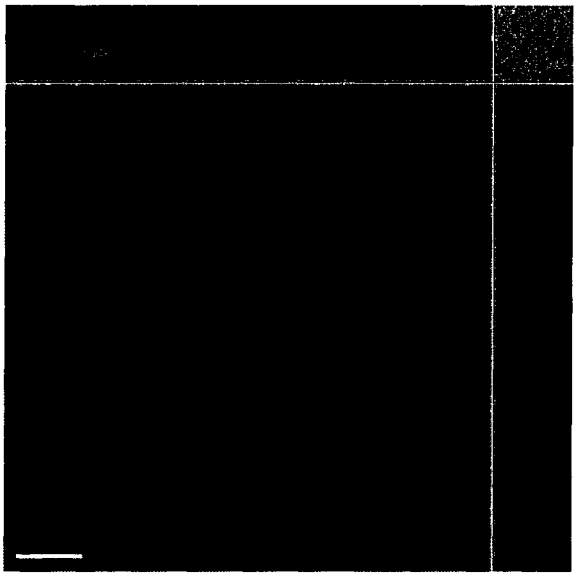

C)

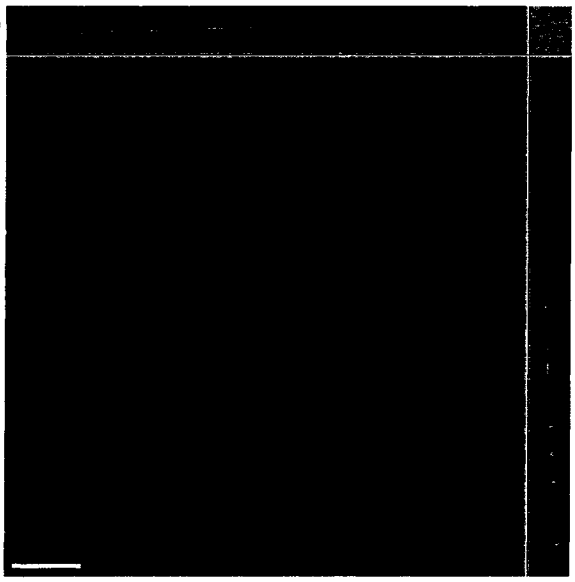

Figure 13, Plate 3.

Day 3

A)

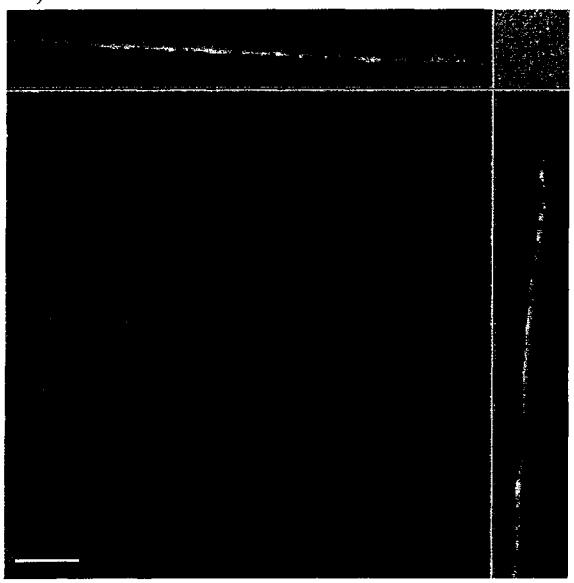

B)

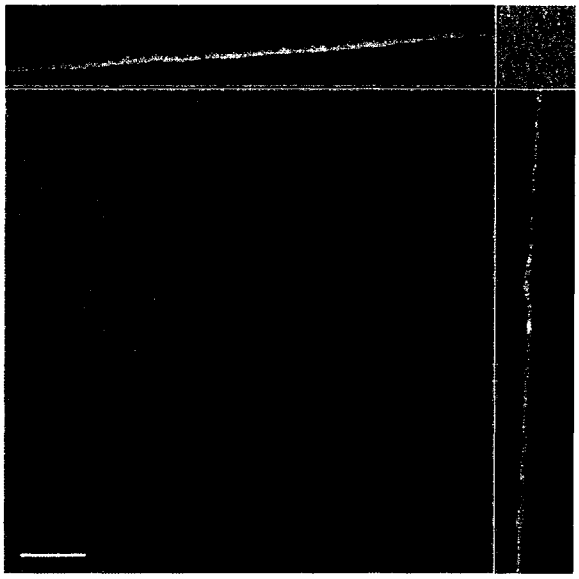

C)

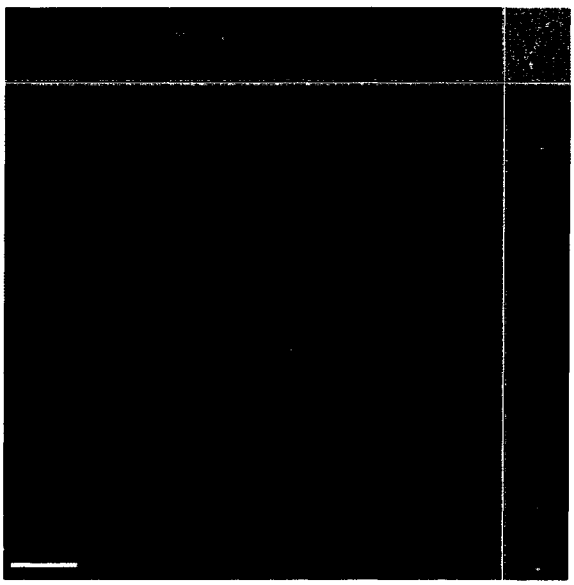

Figure 13, Plate 4.

Day 4

A)

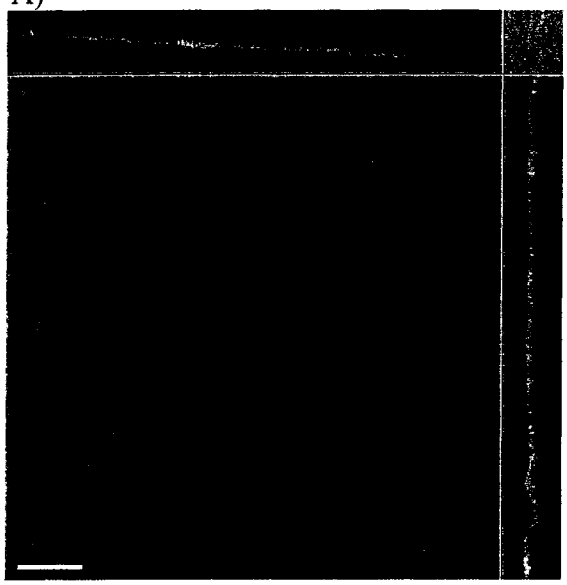

B)

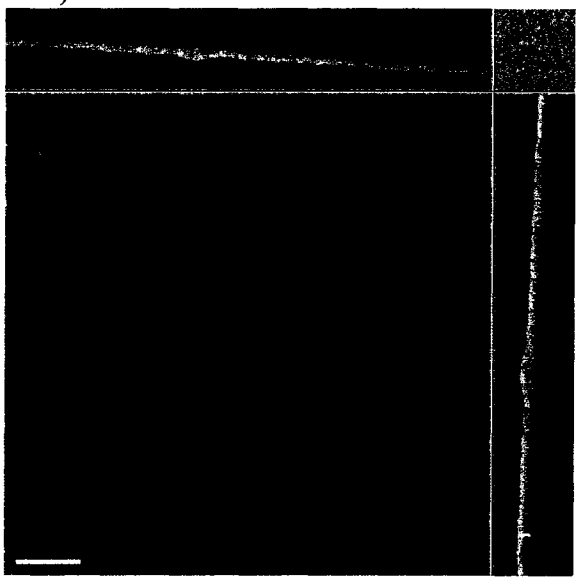

C)

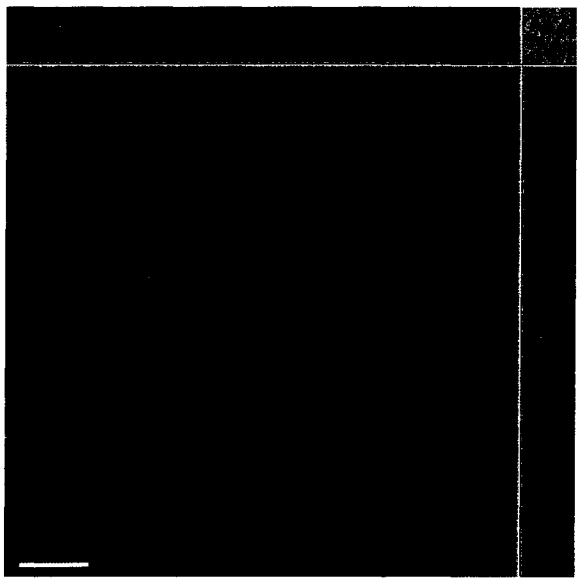

Figure 14, Plate 1. Timecourse of N16961 biofilm development in laminar flow cells. CSLM projections display *gfp*-labeled cells (green) on chitin substratum (red) and glass (red) in *x-y* and selected *x-z* (top), *y-z* (right) saggital sections. Bar = 30 μm.

A) 1h

chitin

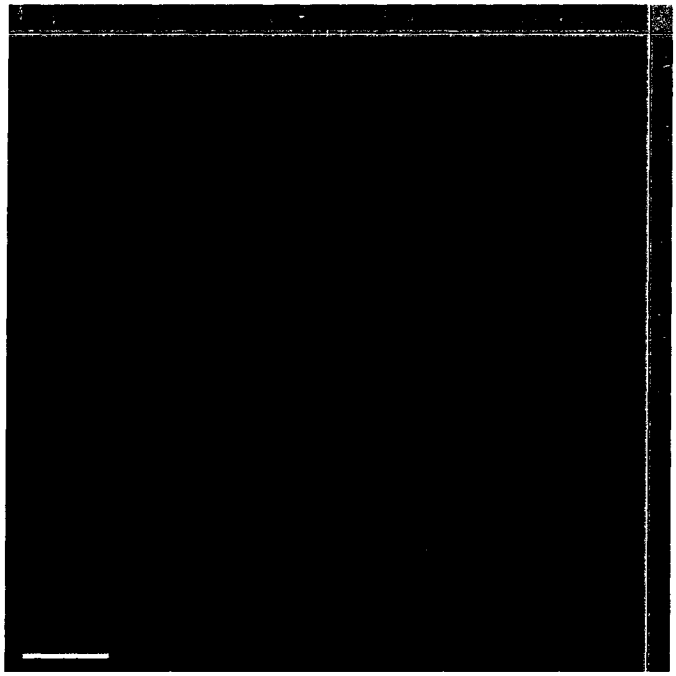

glass

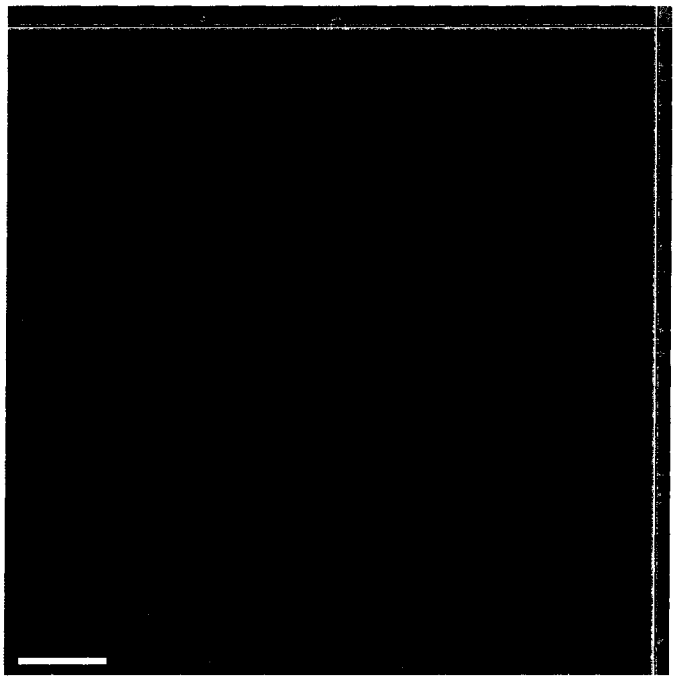

Figure 14, Plate 2.

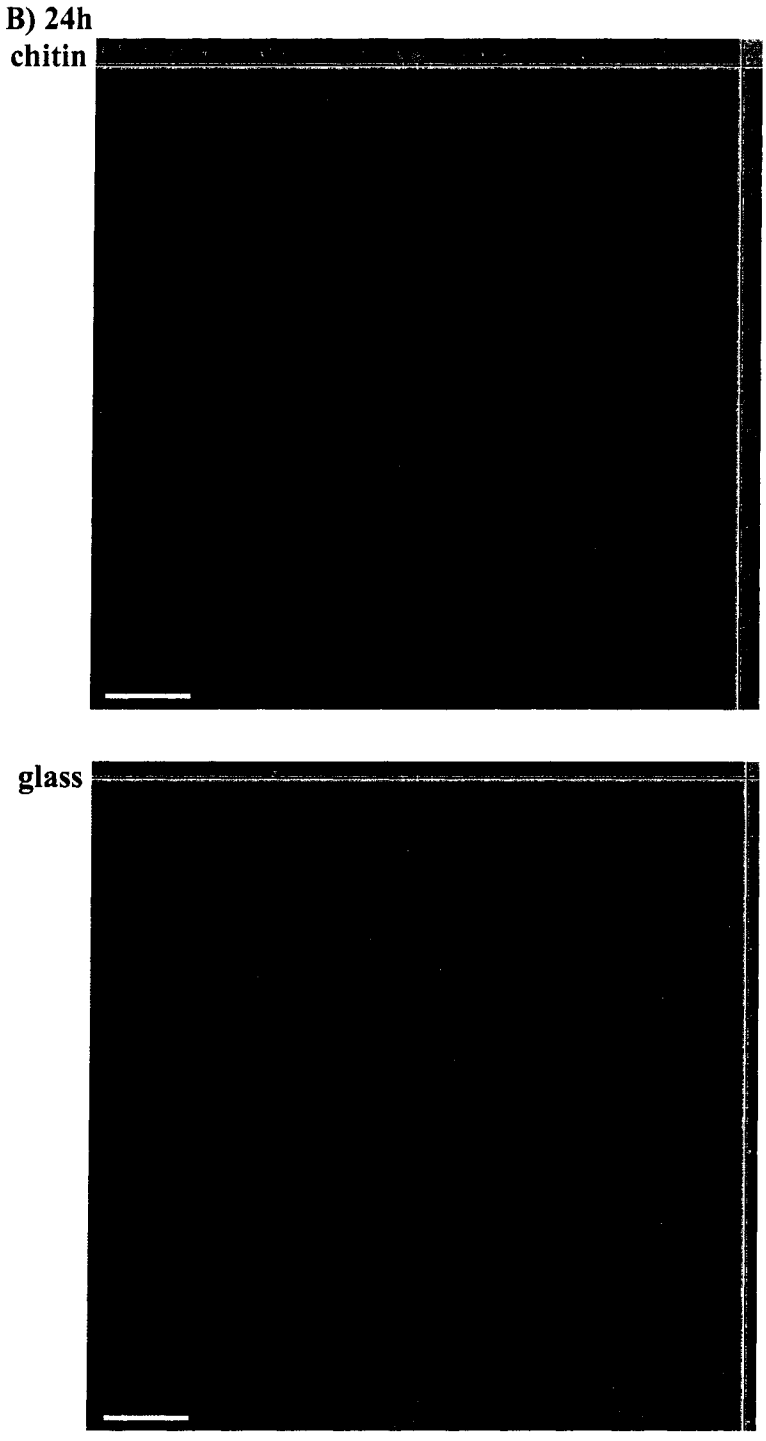

Figure 14, Plate 3.

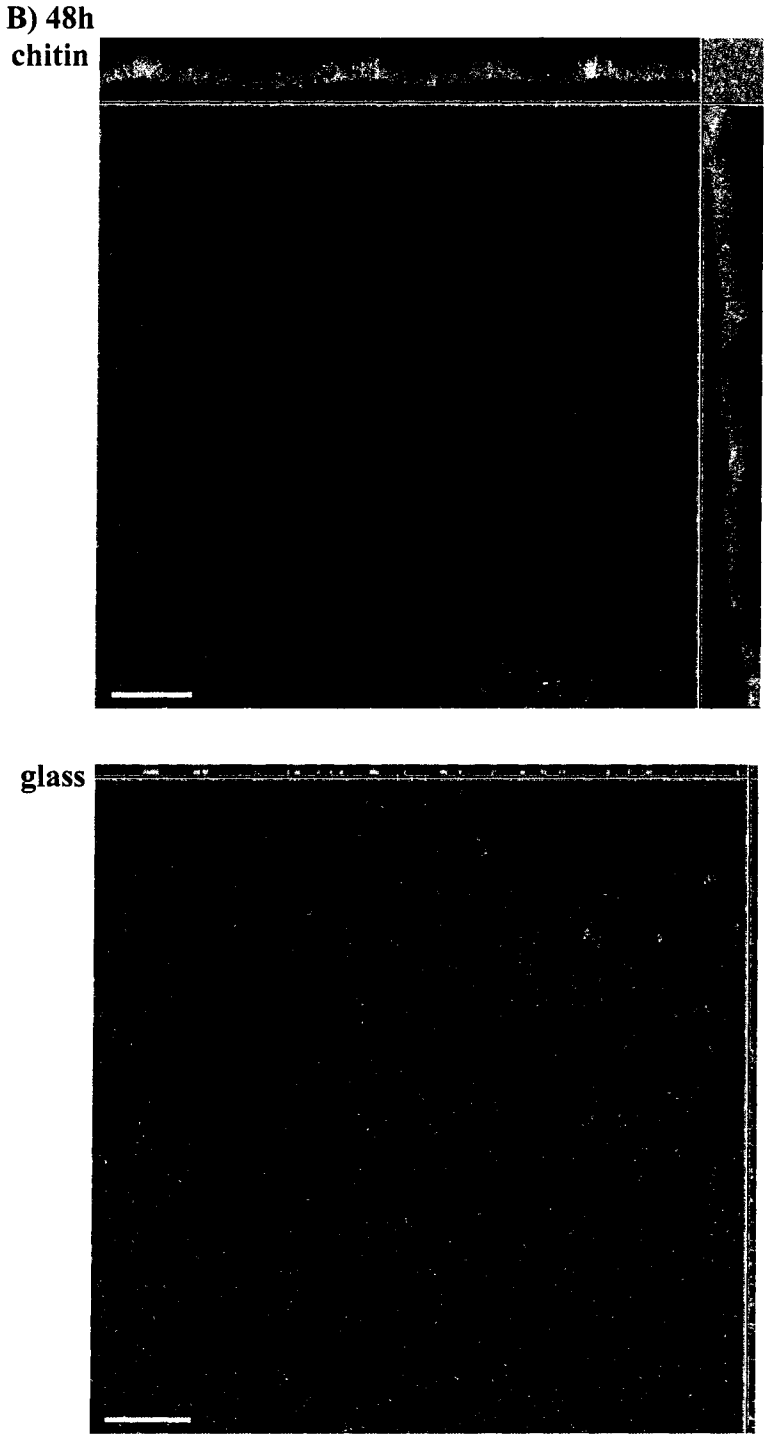

Figure 15. Filamentous N16961 on artificial chitin. Chitin was sampled after 72 hours of incubation in laminar flow cells. Scanning parameters, magnification, and scale bar are shown on the bottom of micrograph. 1 = typical cell, 2 = filamentous cell.